The triple oxygen isotope composition of phytoliths as a proxy of continental atmospheric humidity: insights from climate chamber and climate transect calibrations

Anne Alexandre[1], Amaelle Landais[2], Christine Vallet-Coulomb[1], Clément Piel[3], Sébastien Devidal[3], Sandrine Pauchet[1], Corinne Sonzogni[1], Martine Couapel[1], Marine Pasturel[1], Pauline Cornuault[1], Jingming Xin[2], Jean-Charles Mazur[1], Frédéric Prié[2], Ilhem Bentaleb[4], Elizabeth Webb[5], Françoise Chalié[1], Jacques Roy[3].

[1] CEREGE UM34, Aix-Marseille Université, CNRS, IRD, INRA, Aix en Provence, France
[2] Laboratoire des Sciences du Climat et de l'Environnement (LSCE/IPSL/CEA/CNRS/UVSQ), Gif-sur-Yvette, France
[3]Ecotron Européen de Montpellier, UPS 3248, Centre National de la Recherche Scientifique (CNRS), Campus Baillarguet, Montferrier-sur-Lez, France
[4] ISEM, Université de Montpellier, CNRS, IRD, EPHE, Montpellier, France
[5]Department of Earth Sciences, The University of Western Ontario, London, Ontario,Canada

Correspondance: alexandre@cerege.fr

Abstract

Continental atmospheric relative humidity (RH) is a key climate-parameter. Combined with atmospheric temperature, it allows us to estimate the concentration of atmospheric water vapor which is one of the main components of the global water cycle and the most important gas contributing to the natural greenhouse effect. However, there is a lack of proxies suitable for reconstructing, in a quantitative way, past changes of continental atmospheric humidity. This reduces the possibility to make model-data comparisons necessary for the implementation of climate models. Over the past 10 years, analytical developments have enabled a few laboratories to reach sufficient precision for measuring the triple oxygen isotopes, expressed by the ^{17}O-excess (^{17}O-excess = ln (δ^{17}O + 1) – 0.528 x ln (δ^{18}O + 1)), in water, water vapor and minerals. The ^{17}O-excess represents an alternative to deuterium-excess for investigating relative humidity conditions that prevail during water evaporation. Phytoliths are micrometric amorphous silica particles that form continuously in living plants. Phytolith morphological assemblages from soils and sediments are commonly used as past vegetation and hydrous stress indicators. In the present study, we examine whether changes in atmospheric RH imprint the ^{17}O-excess of phytoliths in a measurable way and whether this imprint offers a potential for reconstructing past RH. For that purpose, we first monitored the ^{17}O-excess evolution of soil water, grass leaf water and grass phytoliths in response to changes in RH (from 40 to 100 %) in a growth chamber experiment where transpiration reached a steady state. Decreasing RH from 80 to 40% decreases the ^{17}O-excess of phytoliths by 4.1 per meg / % as a result of kinetic fractionation of the leaf water subject to evaporation. In order to model with accuracy the triple oxygen isotope fractionation in play in plant water and in phytoliths we recommend direct and continuous measurements of the triple isotope composition of water vapor. Then, we measured the ^{17}O-excess of 57 phytolith assemblages collected from top soils along a RH and vegetation transect in inter-tropical West and Central Africa. Although scattered, the ^{17}O-excess of phytoliths decreases with RH by 3.4 per meg / %. The similarity of the trends observed in the growth chamber and nature supports that RH is an important control of ^{17}O-excess of phytoliths in the natural environment. However, other parameters such as changes in the triple isotope composition of the soil water or phytolith origin in the plant may come into play. Assessment of these parameters through additional growth chambers experiments and field campaigns will bring us closer to an accurate proxy of changes in relative humidity.

1 Introduction

Continental atmospheric relative humidity (RH) is a key climate-parameter. Combined with atmospheric temperature, it allows scientists to estimate the concentration of atmospheric water vapor which is one of the main components of the global water cycle and the most important gas contributing to the natural greenhouse effect (e.g. Held and Soden, 2000; Dessler and Davis, 2010; Chung et al., 2014). However, global climate models (GCMs) have difficulties to properly capture continental humidity conditions (Sherwood et al., 2010; Risi et al., 2012; Fischer and Knutti, 2013). Although tropospheric RH results from a subtle balance between different processes (including air mass origins and trajectories, large scale radiative subsidence, evaporation of falling precipitation, detrainment of convective system, evapotranspiration), it is usually depicted as rather constant in GCMs in agreement with thermodynamic coupling between atmospheric water vapor and sea surface temperature (Bony et al., 2006; Stevens et al., 2017). A model-data comparison approach is thus essential to progress on this issue. This approach has to be applicable beyond the instrumental period to make use of past changes in atmospheric water vapor conditions.

There are multiple ways to reconstruct past continental temperature and precipitation, for instance from pollen (Bartlein et al., 2010; Herbert and Harrison, 2016; Wahl et al., 2012) or tree ring data (Labuhn et al., 2016; Lavergne et al., 2017). However, there is a serious lack of proxies suitable for reconstructing, in a quantitative way, past variations in continental atmospheric RH. Indeed, the stable isotopes of oxygen and hydrogen (δ^{18}O and δD) of tree rings can be influenced by several parameters other than humidity (precipitation source, temperature). This limits the interpretation of tree ring isotope series in terms of humidity changes to places where variations of these other parameters are well constrained (Grießinger et al., 2016; Wernicke et al., 2015). A promising method relies on the δ^{18}O and δD of plant biomarkers (e.g. n-alkanes and fatty acids from leaf waxes) recovered from soils (or buried soils) and sediments. It allows for an estimate in changes in plant water deuterium-excess (d-excess = δD - 8.0 x δ^{18}O), linked to changes in precipitation sources and RH. This method under development can however be biased by factors other than climatic such as plant functional types and selective degradation of the biomarkers (e.g. Rach et al., 2017; Schwab et al., 2015; Tuthorn et al., 2015).

Phytoliths are micrometric amorphous silica (SiO_2, nH_2O) particles that form continuously in living plants. Silicon is actively absorbed by the roots (Ma and Yamaji, 2006) and is translocated in the plant tissues where it polymerizes inside the cells, in the cell walls and in extracellular spaces of stems and leaves. Silica polymerization appears to be an active physiological process, which does not only depends on transpiration (Kumar et al., 2017). In grasses, which are well known silica accumulators, silica accounts for several % of dry weight (d.w.) and is mainly located in the stem and leaf epidermis. Phytolith morphological assemblages from soils and sediments are commonly used as past vegetation and hydrous stress indicators (e.g. Aleman et al., 2012; Backwell et al., 2014; Bremond et al., 2005a, 2005b; Contreras et al., 2014; Nogué et al., 2017 ; Piperno, 2006). The potential of the $\delta^{18}O$ signature of phytoliths ($\delta^{18}O_{Phyto}$) from grasses for paleoclimate reconstruction has been investigated through growth chamber and North American Great Plains calibrations. It has been shown that the $\delta^{18}O_{Phyto}$ of grass stems weakly affected by transpiration correlated with the $\delta^{18}O$ signature of soil water ($\delta^{18}O_{SW}$) and the atmospheric temperature, as expected for a polymerization of silica in isotope equilibrium with the plant water (Webb and Longstaffe, 2000, 2002, 2003, 2006). It has also been shown that $\delta^{18}O_{Phyto}$ from grass leaves correlated with RH as expected for an evaporative kinetic isotope enrichment of the leaf water (e.g. Cernusak et al., 2016) imprinted on $\delta^{18}O_{Phyto}$. However, because grass stem and leaf phytoliths have the same morphology and are mixed in soil and sedimentary samples, these calibrations were not sufficient for using $\delta^{18}O_{Phyto}$ of grassland phytolith assemblages as a paleoclimatic signal. In tropical trees, silica is found in leaves, bark and wood and accounts for a few % d.w. (e.g. Collura and Neumann, 2017). In the wood, silica polymerizes in the secondary xylem supposedly unaffected by transpiration, in the form of Globular granulate phytolith types (Madella et al., 2005; Scurfield et al., 1974; Welle, 1976). These phytoliths make up more than 80% of tropical humid forest and rainforest phytolith assemblages found in soils and sediments (Alexandre et al., 2013; Collura and Neumann, 2017; Scurfield et al., 1974; Welle, 1976). Examination of the $\delta^{18}O_{Phyto}$ of rainforest assemblages showed correlations with the $\delta^{18}O$ of precipitation ($\delta^{18}O_{Pre}$) and the atmospheric temperature (Alexandre et al., 2012). However, in this case, the use of $\delta^{18}O_{Phyto}$ did not further develop because it was applicable only to forested areas and humid climatic periods, which is a major drawback for paleoclimatic reconstructions.

The triple isotope composition of oxygen in the water molecule represents an alternative for investigating RH conditions prevailing during water evaporation. In the triple isotope system, the mass-dependent fractionation factors between A and B (${}^{17}\alpha_{A–B}$ and ${}^{18}\alpha_{A–B}$) are related by the exponent $\theta_{A–B}$ (${}^{17}\alpha_{A–B} = {}^{18}\alpha_{A–B}{}^{\theta}$ or $\theta_{A–B} = \ln{}^{17}\alpha_{A–B} / \ln{}^{18}\alpha_{A–B}$). The exponent can also be expressed as $\theta_{A–B} = \Delta'^{17}O_{A–B} / \Delta'^{18}O_{A–B}$ with $\Delta'^{17}O_{A–B} = \delta'^{17}O_{A}-\delta'^{17}O_{B}$, $\Delta'^{18}O_{A–B} = \delta'^{18}O_{A}-\delta'^{18}O_{B}$, $\delta'^{17}O = \ln(\delta^{17}O + 1)$ and $\delta'^{18}O = \ln(\delta^{18}O + 1)$. In the $\delta'^{17}O$ vs $\delta'^{18}O$ space, $\lambda_{A–B}$ represents the slope of the data alignment during mass-dependent fractionation between A and B. Whereas $\theta_{A–B}$ is linked to a particular physical process (equilibrium or kinetic), $\lambda_{A–B}$ is empirically measured between two groups of materials and is not related to a well-understood single process (Pack and Herwartz, 2014). It has been recently estimated that θ equals 0.529 for liquid-vapor equilibrium (θ_{equil}; Barkan and Luz, 2005) and 0.518 for vapor diffusion in air (Barkan and Luz, 2007). It has additionally been shown that meteoric waters plot along a trend with a slope λ of 0.528 ± 0.001. The departure from this trend is conventionally called ^{17}O-excess (^{17}O-excess = δ'^{17}O - 0.528 x δ'^{18}O) (Luz and Barkan, 2010). In case of mass-dependent fractionation processes, the magnitudes of the ^{17}O-excess in waters and minerals are very small and measurement of the ^{17}O-excess, expressed in per meg (10^{-3} ‰), requires very high analytical precisions.

In the water cycle, the ^{17}O-excess variations mainly result from diffusion processes, while equilibrium fractionation does not lead to important departure from the meteoric water mean trend. Theoretical and empirical estimations have shown that in contrast to d-excess, and except at very high latitudes, changes in water ^{17}O-excess are not significantly impacted by temperature (~0.1 per meg / °C ; Uemura et al., 2010) and much less sensitive to distillation processes (Angert et al., 2004; Barkan and Luz, 2007; Landais et al., 2008; Uemura et al., 2010; Steig et al., 2014). Changes in water ^{17}O-excess are thus essentially controlled by evaporative kinetic fractionation. The ^{17}O-excess decreases in the evaporating water and increases in the vapor phase when RH decreases at evaporative sites (e.g. sea surface, lake surface, soil surface or leaf surface). Over the last ten years, a few studies used the ^{17}O-excess of water to interpret ice core archives in climatic terms (Guillevic et al., 2014, Schoeneman et al., 2014; Winkler et al., 2012; Landais et al., 2008, 2012). They supported that ^{17}O-excess is a marker of RH, sea-ice extent at the moisture source, and air mass mixing (Risi et al., 2010) except at the very high latitudes of East Antarctica where temperature can have a significant influence. The observed variations of ^{17}O-excess in Greenland ice cores of ~20 per meg maximum were thus interpreted as variations of RH or sea-ice extent at the source region and coincide with variations in the low to mid latitude water cycle as recorded by other proxies (such as CH_4 or δD of CH_4) (Guillevic et al., 2014). An even smaller number of studies measured or attempted to model the ^{17}O-excess of rainwater at low and temperate latitudes (Affolter et al., 2015; Landais et al., 2010b; Li et al., 2015; Luz and Barkan, 2010; Risi et al., 2013). The observed variations in ^{17}O-excess, partly explained by convective processes and re-evaporation of precipitation, were of the order of 30-40 per meg, either during a rainy event or along climatic gradients. Only two studies focused on open surface waters, and showed that variations of the ^{17}O-excess ranged from tens to hundreds of per meg when the surface water underwent strong evaporative enrichment (Surma et al., 2015; Luz and Barkan, 2010), in agreement with the Craig and Gordon (1965) formulation. The most important variations in ^{17}O-excess occur at the plant-atmosphere interface. In leaf water, variations higher than 200 per meg were encountered (Landais et al., 2006; Li et al., 2017). Difference in ^{17}O-excess between leaf water subject to evaporation (LW) and stem water (SW) not subject to evaporation, increased with decreasing RH (from 100 to 30 %), as expected for processes dominated by kinetic fractionation. When measuring a sequence of LW- SW couples sampled under different climatic conditions, the slope of the line linking their triple isotope composition and named λ_{transp}, equivalent to $\lambda_{LW\text{-}SW}$, was found to change with RH. This pattern was neither influenced by the plant species nor by the environmental conditions (e.g. atmospheric temperature, soil water conditions) (Landais et al., 2006). However opposite trends of λ_{transp} with RH were observed from one study to another (Landais et al., 2006; Li et al., 2017). This discrepancy was attributed to the possibility that steady state is not always reached during sampling and to likely differences in isotope composition of the ambient vapor, a parameter of the Craig and Gordon model that is often not measured but estimated (Li et al., 2017).

While ^{17}O-excess measurements of waters were expanding, analyses of the triple oxygen isotope composition of minerals (mostly silicates and carbonates) were also developed, allowing estimate of fractionation during polymerization and providing constraints on both temperature and isotope composition of the water source (Pack and Herwartz, 2014; Levin et al., 2014; Passey et al., 2014; Herwartz et al., 2015; Miller et al., 2015; Sharp et al., 2016). Variations of ^{17}O-excess of the order of tens to hundreds of per meg were reported from one mineral to another. For most of the studies cited above, the objective was to discriminate between high and low temperature formation processes or to decipher from which type of water the mineral formed (i.e. sea water, hydrothermal water, meteoric or surface water). The ^{17}O-excess of biogenic and sedimentary carbonates was also investigated as a potential record of evaporating water sources (Passey et al., 2014).With regard to silicate-water fractionation, the relationship between the three oxygen isotopes defined by $\theta_{\mathrm{SiO2\text{-}water}}$ was estimated between 0.521 and 0.528, increasing logarithmically with temperature (Sharp et al., 2016).

In the present study, in the light of the recent findings cited above, we examined whether changes in atmospheric RH imprint the ^{17}O-excess of phytoliths (^{17}O-excess$_{\mathrm{Phyto}}$) in a measurable way and whether this imprint offers a potential for reconstructing past RH. For that purpose, we first monitored the ^{17}O-excess evolution of soil water, grass leaf water and grass phytoliths in response to changes in RH in a growth chamber experiment. Then, we measured the ^{17}O-excess$_{\mathrm{Phyto}}$ from 57 phytolith assemblages collected in soil tops along a RH and vegetation transect in inter-tropical West and Central Africa. Relationships between ^{17}O-excess$_{\mathrm{Phyto}}$ and RH were looked for and assessed on the basis of previous quantifications of kinetic isotope enrichment of leaf water and equilibrium fractionation between water and silica. Results from the natural sampling were compared to the ones from the growth chamber experiment to evaluate the importance of RH in controlling ^{17}O-excess$_{\mathrm{Phyto}}$ in natural environment.

2 Materials and methods

2.1 Samples from the growth chamber experiment

Festuca arundinacea, commonly referred to as tall fescue, is widely distributed globally as forage and an invasive grass species (Gibson and Newman, 2001) and can adapt to a wide range of conditions. In 2016, *F. arundinacea* (Callina RAGT Semences) was grown in three chambers under three conditions of RH (ca. 40, 60 and 80 %) kept constant using wet air introduction and ultrasonic humidifier. We checked that the humidifiers did not lead to any isotope fractionation between the water in their reservoirs and the vapor delivered. Temperature and light intensity were kept constant at 25 ± 0.6 (standard deviation (SD)) °C and 293 ± 14 (SD) mmol / m^2 / sec respectively.

In a 35 L tank (53 x 35 x 22 cm), 20 kg of dried commercial potting soil were packed above a 1.6

cm layer of quartz gravel. A porous cup for water extraction was placed in the soil with its extraction tube hermetically extending outside of the tank walls. The soil was irrigated with 10 L of the same water as the one used for the humidifier. Four grams of seeds were sown along four rows in each tank, resulting in about 6000 seedlings. Each tank was then placed in a chamber and was irrigated from a Mariotte bottle (25 L) placed next to it. The Mariotte system was set so that a water saturated level of 5 cm remained constant at the base of the tank. The irrigation water was supplemented with 105 mg/L of SiO_2 (in the form of SiO_2 K_2O). Ten days after germination, agar-agar (polysaccharide agarose) was spread on the soil surface around the seedlings (about 8 cm tall), to prevent any evaporation (Alexandre et al., 2016).

A fourth tank was kept at 100% of RH thanks to the installation of a 20 cm high plexiglass cover, in a forth chamber set at 80 % of RH. In this case no agar-agar was added and the vapor around *F. arundinacea* came from evaporation and transpiration of the soil water. Otherwise the treatment was the same as in the other chambers.

For each humidity condition, three to four harvests were made at intervals of 10-14 days. The 20-25 cm long leaves were cut at two cm above the soil level and weighed. From the first to the fourth sampling, the harvested wet leaves increased from 15-20 g (10 days of growth) to 40-60 g (14 days of growth). Three to five g of leaves were put in glass gastight vials and kept frozen for bulk leaf water extraction. The remaining leaves were dried for phytolith extraction. Forty mL of irrigation water from the Mariotte bottle, and of soil water from the porous cup, were kept at 5°C before analyses.

After each harvest, the tanks were left in their chamber of origin but the 40, 60 and 80 % RH treatments were rotated between the growth chambers so that the four replicates of a given RH treatment would come from at least two different chambers. The 100 % humidity was set up in a unique chamber during the entire duration of the experiment. The harvested leaves in this treatment were often covered by condensation drops which were blotted between two sheets of wiping paper, rapidly after harvesting. The experimental setup details and the harvest list are given in table 1.

2.2 Samples from the natural climate transects

Fifty-seven top soil samples were collected during several field trips along vegetation and humidity transects in Mauritania and Senegal (Bremond et al., 2005b ; Lézine, 1988; Pasturel, 2015) (Lezine, 1988) Gabon (Lebamba et al., 2009) and Congo (Alexandre et al., 1997) in the saharan, sahelian, sudanian, guinean and congolian bioclimatic zones, respectively (White et al., 1983). Samplings, phytolith extractions and phytolith morphological assemblages descriptions are given in the above-mentioned studies, except for the samples of Gabon from which phytoliths were chemically treated and counted in the frame of the present study.

The sampled site location as well as the associated climatic and oxygen isotope variables are given in Table 2. The vegetation overlying the sampled soils was categorized into savanna (Mauritania, Senegal), wooded savanna (Senegal), humid forest (Gabon and Congo) and enclosed savanna (Gabon). For each sampled site, yearly climate average were calculated from the monthly means of temperature, precipitation, RH and diurnal temperature, extracted from the Climate Research Unit (CRU) 1961 - 1990 time series (10' spatial resolution; http://www.cru.uea.ac.uk, Harris et al., 2013, CRU 2.0). Mean Annual Precipitation (MAP), Mean Annual Temperature (MAT) and mean annual RH range from 49 to 2148 mm, 24.3 to 29.8 °C and 40.2 to 82.5 %, respectively. In addition, in order to get a proxy of RH during wet months, likely those of the grass growing season, averaged RH monthly means for months with at least one day with precipitation higher than 0.1 mm (RH-rd0>1) was calculated. It ranges from 56.3 to 82.5 %. As maximum transpiration is supposed to be reached around 15:00 UTC we also calculated RH and RH-rd0>1 at 15:00 (RH15 and RH15-rd0>1, respectively) according to New et al. (2002) and Kriticos et al. (2012). For each sampling site, estimates of $\delta'^{18}O$ of precipitation for the months with at least one day with precipitation higher than 0.1 mm ($\delta'^{18}O_{Pre\text{-}rd0>1}$) were calculated from $\delta^{18}O$ of precipitation extracted from The Online Isotopes in Precipitation Calculator-version OIPC2-2 (http://www.waterisotopes.org; Bowen and Revenaugh, 2003; Bowen and Wilkinson, 2002; Bowen et al., 2005) and weighted by the amount of precipitation. The estimates range from -1.51 to -4.46 ‰. There is currently no data on the ^{17}O-excess of precipitation ($^{17}O\text{-excess}_{Pre}$) at these sites.

2.3 Phytolith chemical extractions

Phytoliths from soils were extracted following Crespin et al. (2008) using HCl, H_2O_2, $C_6H_5Na_3O_7$ and $Na_2O_4S3\text{-}H_2O$ at 70 °C, and a $ZnBr_2$ heavy liquid separation. It has been shown that up to a temperature of 70 °C the extraction has no effect on the $\delta^{18}O$ (Crespin et al., 2008). We verified that it did not have any effect on the ^{17}O-excess either, using our internal standard MSG extracted at 60 and 70°C (Crespin et al., 2008). The obtained ^{17}O-excess values were similar (-211 and -243 per meg, respectively) given our reproducibility of ±34 per meg (see section 2.6.1). Phytoliths from *Festuca arundinaceae* were thus extracted using a high purity protocol with HCl, H_2SO_4, H_2O_2, HNO_3, $KClO_3$ and KOH at 70 °C following Corbineau et al. (2013).

2.4 Phytolith counting

Phytolith assemblages from the humidity transects were mounted on microscope slides in Canada Balsam, for counting, at a 600X magnification. More than 200 identifiable phytoliths with a diameter greater than 5 µm and with a taxonomic significance were counted per sample. Three repeated counting gave an error of ± 3.5 % (SD). Phytoliths were named using the International Code for Phytolith Nomenclature 1.0 (Madella et al., 2005) and categorized as Globular granulate type produced by the wood (Scurfield et al., 1974; Kondo et al., 1994), palm Globular echinate type and grass types comprising Acicular, Bulliform, Elongate psilate, Elongate echinate, Bulliform cells, and Grass Short Cells types. For each sample from the natural transects, the phytolith index d/p, a proxy of tree cover density (Alexandre and Bremond, 2009; (Bremond et al., 2005b), was calculated. It is the ratio of Globular granular phytolith category (Madella et al., 2005) formed in the secondary xylem of the dicotyledon (d) wood to the grass short cell phytolith category formed in the epidermis of grasses or Poideae (p) (Collura and Neumann, 2017; Scurfield et al., 1974; Welle, 1976). Those two categories make up most of the phytolith assemblages recovered from inter-tropical soils (Bremond et al., 2005b, 2005a)Alexandre et al., 1997, 2013; Bremond et al., 2005b, 2005a).

Phytolith assemblages from the *F. arundinacea* samples were also mounted and counted. The phytolith types were categorized according to their cell of origin in the epidermis into Epidermal short cell, Epidermal long cell, Bulliform cell and Hair acicular.

2.5 Leaf and soil water extraction

Leaf water was extracted using a distillation line. Leaves were introduced in a glass tube connected to the distillation line, and frozen through immersion of the glass tube in liquid nitrogen. While keeping the sample frozen, the distillation line was pumped to reach a vacuum higher than 5.10^{-2} mbar. The pumping system was then isolated and the glass sample tube warmed to 80°C. Meanwhile, at the other end of the distillation line, a glass collecting tube was immersed in liquid nitrogen to trap the extracted water. To avoid condensation, the line between the sample tube and the collection tube was heated with a heating wire. The distillation was completed after six hours. In order to remove volatiles from the extracted water, a few granules of activated charcoal were added and the water slowly stirred for 12 h.

Soil water was extracted using a 31mm porous ceramic cup. Brown or yellow-colored samples were filtered at 0.22µm, but remained colored after filtration, indicating the presence of soluble compounds.

2.6 Isotope analyses

The oxygen isotope results are expressed in the standard δ-notation relative to VSMOW.

2.6.1 Phytoliths

Phytolith samples of 1.6 mg were dehydrated and dehydroxylated under a flow of N_2 (Chapligin et al., 2010) and oxygen extraction was performed using the IR Laser-Heating Fluorination Technique at CEREGE (Aix-en-Provence, France) (Alexandre et al., 2006, Crespin et al., 2008; Suavet et al., 2010). The purified oxygen gas (O_2) was passed through a −114 °C slush to refreeze gases interfering with the mass 33 (e.g. NF), potentially produced during the fluorination of residual organic N, before being sent to the dual-inlet mass spectrometer (ThermoQuest Finnigan Delta Plus). The composition of the reference gas was determined through the analyses of NBS28 for which isotope composition has been set to $\delta^{18}O$=9.60 ‰, $\delta^{17}O$=4.99 ‰ and ^{17}O-excess = -65 per meg. During the measurement period, reproducibility (SD) of the analyses of the working quartz standard (Boulangé 2008) against which the isotope composition of the sample gas was corrected on a daily basis (3 quartz standards were analysed per day) was ± 0.20 ‰, ± 0.11 ‰ and ± 22 per meg for $\delta^{18}O$, $\delta^{17}O$ and ^{17}O-excess respectively (n = 63; one run of eight dual inlet measurements). For every session of measurement, the effectiveness of the entire dehydration and IR-Laser-Fluorination-IRMS procedure was checked through the analysis of a working phytolith standard (MSG60) with $\delta^{18}O$ = 36.90 ± 0.78 ‰, $\delta^{17}O$ = 19.10 ± 0.40 ‰ and ^{17}O-excess = -215 ± 34 per meg (n = 29). For comparison, the inter-laboratory pooled value for MSG60 is $\delta^{18}O$ = 37.0

± 0.8 ‰ (Chapligin et al., 2011). Recent measurements of the silicate reference materials UWG-2 garnet (Valley et al., 1995) and San Carlos (SC) olivine gave the following values: $\delta^{18}O_{UWG-2}$ = 5.72 ± 0.12 ‰, $\delta^{17}O_{UWG-2}$ = 2.95 ± 0.06 ‰, ^{17}O-excess$_{UWG-2}$ = -68 ± 27 per meg (n = 5), $\delta^{18}O_{SC}$ = 4.95 ± 0.22 ‰, $\delta^{17}O_{SC}$ = 2.56 ± 0.12 ‰, ^{17}O-excess$_{SC}$ = -49 ± 24 per meg (n = 3). For comparison, silicate analyses presented in Sharp et al. (2016) are normalized to a δ^{18}O value for San Carlos Olivine of 5.3 ‰ and a ^{17}O-excess value of -54 per meg. As previously discussed in Suavet et al. (2010), a large scatter is often observed for SC olivine δ^{18}O and δ^{17}O values measured in a given laboratory or from a laboratory to another. This is probably attributable to the heterogeneity of the analyzed samples. At CEREGE, the internal standard of SC olivine is prepared from a number of millimetric crystals with possibly different oxygen isotope composition. The δ^{18}O and δ^{17}O values from Suavet et al. (2010), Tanaka and Nakamura (2013) Pack et al. (2016), Sharp et al. (2016) and the present study average 5.29 ± 0.23 (1 SD) ‰ and 2.72 ± 0.12 (1 SD) ‰, respectively. Nevertheless, despite the large SD on ^{18}O and δ^{17}O measurements, the SC olivine ^{17}O-excess appears relatively constant (-71 ± 23 (1 SD)) per meg.

2.6.2 Leaf water

Leaf water was analyzed at LSCE (Gif sur Yvette, France) following the procedure previously detailed in Landais et al. (2006). In summary, a fluorination line was used to convert water to oxygen using CoF_3 heated at 370°C in a helium flow. The oxygen was then trapped in a tube immersed in liquid helium before being analyzed by dual inlet IRMS (ThermoQuest Finnigan MAT 253 mass spectrometer) against a reference oxygen gas. All measurements were run against a working O_2 standard calibrated against VSMOW. The resulting precisions (2 runs of 24 dual inlet measurements) were 0.015 ‰ for δ^{17}O, 0.010 ‰ for δ^{18}O and 5 per meg for ^{17}O-excess.

2.6.3 Irrigation and soil waters

Irrigation and soil water were analyzed at the Ecotron of Montpellier (France) with an isotope laser analyzer (Picarro L2140i) operated in ^{17}O-excess mode using an auto-sampler and a high precision vaporizer. Each water sample was used to fill three vials randomly dispatched in four groups of six samples (three replicates per sample). Each sample group was bracketed by three working standards (Giens-1, Iceberg-1 and Eco-1). Ten injections were performed for each vial, and the results of the first six injections were discarded to account for memory effects. Following IAEA recommendations (IAEA, 2013), each liquid measurement sequence was started with two vials of deionized water for instrument conditioning.

The isotope compositions of each sample group were calibrated using the three interpolated mean values obtained for the bracketing working standards (Delattre et al., 2015). All isotope ratios were normalized on the VSMOW2/SLAP2 scale, with an assigned SLAP2 ^{17}O-excess value of zero, following the recommendations of Schoenemann et al. (2013). The resulting precisions (3 replicates) were 0.02 ‰, 0.01 ‰ and 10 per meg for δ^{17}O, δ^{18}O and ^{17}O-excess (n=31).

The three working standards were also analyzed using the fluorination/IRMS technique used for leaf water analyses at LSCE. The ^{17}O-excess maximum difference was 6.4 per meg, which is lower than the analytical precision obtained using the laser spectrometer (Table S1a).

In order to assess that soluble organic compounds present in some soil water samples did not impact the laser analyzer isotope measurements (Martín-Gómez et al., 2015), a representative set of colored samples were analyzed with and without the Picarro micro combustion module (MCM) set up between the high precision vaporizer and the analyzer inlet. This system was designed to partly remove organic volatile compounds using a catalytic process. The obtained isotope compositions were not significantly different (Table S1b), suggesting that organic compounds were either in low concentration, and/or did not interfere in the spectral window used by the analyzer. Therefore, the other soil water samples were analyzed without the MCM.

3 Results

3.1 Growth chamber experiment

δ'^{18}O and ^{17}O-excess of the irrigation water (respectively $\delta'^{18}O_{IW}$ and ^{17}O-excess$_{IW}$) average -5.59 ± 0.00‰ and 26 ± 5 per meg, respectively. δ'^{18}O and ^{17}O-excess of the soil water (respectively $\delta'^{18}O_{SW}$ and ^{17}O-excess$_{SW}$) average -2.89 ± 0.19 ‰ and 16 ± 8 per meg, respectively (table S2). The isotope difference is thus significant for δ'^{18}O, less significant for ^{17}O-excess, according to the analytical error. Although evaporative kinetic fractionation of the top soil water suctioned by the porous cup under vacuum cannot be ruled out, isotopic exchanges between the soil water and oxygen-bearing phases of the rhizosphere may also have impacted the soil water isotopic composition (Bowling et al., 2017; Chen et al., 2016; Oerter et al., 2014; Orlowski et al., 2016). Hereinafter, we consider the isotope signatures of the water absorbed by the roots of *F. arundinacea* to be equivalent to the irrigation water that fed the saturation level at the base of the tank. This water was reached by the deepest roots, as observed on a cross-section of the soil after the end of the experiment, and likely reached the upper roots by capillarity.

The transpiration of *F. arundinacea* increases rapidly from 0.03 to 0.6 L / day from 100 to 60 % RH and more slowly from 60 to 40 % RH where it reaches 0.61 L / day (averages of the replicates, Table 1). In response to decreasing RH, δ'^{18}O (table S2) and ^{17}O-excess (fig. 1a) values of the bulk leaf water ($\delta'^{18}O_{LW}$ and ^{17}O-excess$_{LW}$) show clear increasing and decreasing trends, respectively. The averaged ^{18}O-enrichment of bulk leaf water relatively to irrigation water ($\Delta'^{18}O_{LW-IW}$) increases from 100 to 60 % of RH and seems to be stabilizing from 60 to 40 % RH (fig. 1b; Table 1). For 100 % RH, the high standard deviations (SD) associated with $\delta^{18}O_{LW}$ (table S2), and consequently with $\Delta'^{18}O_{LW-IW}$ (Table 1), are due to the very high $\delta^{18}O_{LW}$ value of sample P3-100-10-05-16. However, as we do not have any explanation for this high value, this data was not excluded from further calculation. The ^{17}O-excess values associated with the enrichment $\Delta'^{18}O_{LW-IW}$ (or ^{17}O-excess$_{e\ LW-IW} = \Delta'^{17}O_{LW-IW} - 0.528 \times \Delta'^{18}O_{LW-IW}$) are scattered for a given RH. The averaged value however follows a clear pattern (fig. 1c; table 1): it decreases slowly from 100 to 80 % RH (from -88 ± 48 to -75 ± 20 per meg,) and more rapidly from 80 to 40% RH where it reaches -159 ± 9 per meg. When the relationship is linearized, the slope of the line between ^{17}O-excess$_{e\ LW-IW}$ and 40 to 80 % RH is 2.3 per meg/% (fig. 1f). The raw values of λ_{LW-IW} do not show any significant trend with RH and average 0.519 ± 0.002 (table 1).

The average phytolith content ranges from 1.1 to 0.1% d.w. Silicification of the leaf blade of *F. arundinacea* increases with increasing transpiration and decreasing humidity (Table 1). Phytolith morphological identification shows that they formed preferentially in the epidermal short cell and to a smaller extent in the epidermal long cells (fig. 2). The proportion of silicified long cells, increases with increasing transpiration and decreasing RH (Table 1). Some hair and bulliform cells were also silicified, but in much smaller quantities. δ'^{18}O and ^{17}O-excess of phytoliths (δ'^{18}O$_{Phyto}$ and ^{17}O-excess$_{Phyto}$ respectively) show the same general trends with RH as δ'^{18}O$_{LW}$ and ^{17}O-excess$_{LW}$ (fig. 1a, table S2).

The average value of the ^{18}O-enrichment of phytoliths relative to the bulk leaf water (Δ'^{18} O$_{Phyto-LW}$) increases slowly (from 27.97 ± 6.97 to 28.47 ± 0.38‰) when RH decreases from 100 to 80 % and more rapidly from 80 to 40% where it reaches 32.32 ± 1.92 ‰ (fig. 1b, Table 1). With regard to the enrichment of phytoliths relative to the irrigation water, Δ'^{18}O$_{Phyto-IW}$ shows the same trend with RH as Δ'^{18}O$_{LW-IW}$ (fig.1b, table 1). ^{17}O-excess$_{Phyto}$ and ^{17}O-excess$_{e\ Phyto-IW}$ shows the same decreasing trend with RH as ^{17}O-excess$_{e\ LW-IW}$ (fig. 1c, Table 1). When the relationships of ^{17}O-excess$_{Phyto}$ and ^{17}O-excess$_{e\ Phyto-IW}$ with 40 to 80 % RH are linearized, the slopes of the lines are 4.1 and 4.3 per meg/%, respectively (fig. 1d, 1f). A Student's t-test (relevant when the variance of two data sets are equal; Andrade and Estévez-Pérez, 2014), calculated on the ^{17}O-excess$_{e\ LW-IW}$ *vs* RH and ^{17}O-excess$_{e\ Phyto-IW}$ *vs* RH data sets shows that the slopes of the lines are not statistically different for a 75% confidence interval. Thus, the link between ^{17}O-excess$_{e\ Phyto-IW}$ and RH is mainly due to the leaf water ^{17}O-excess dependency to RH. The raw values of $\lambda_{Phyto-LW}$ appears constant, averaging 0.522 ± 0.001 (table 1).

3.2 Natural samples

Values of δ'^{18}O$_{Phyto}$ and ^{17}O-excess$_{Phyto}$ range respectively from 23.79 to 38.16 ‰ and from -140 to -290 per meg (table 2). The variations are in the same order of magnitude as for the growth chamber experiment. The estimates of δ^{18}O$_{Pre}$ vary little along the sampled transect (from -4.46 to –3.22 ‰). No relationship is observed between δ'^{18}O$_{phyto}$ or the ^{18}O-enrichment of phytoliths relatively to precipitation (Δ'^{18}O$_{Phyto-Pre}$) and MAP, MAT or RH (fig. 3, table 2).

Although scattered, the ^{17}O-excess$_{Phyto}$ values show a significant positive linear correlation with RH (fig. 4), regardless of which RH variable is taken into account. After excluding two outliers, the slopes of the correlation lines are 2.1 and 2.2 when RH and RH15 are taken into account, 3.4 when either RH-rd0>1 or RH15-rd0>1 are considered. The relationship obtained between ^{17}O-excess$_{Phyto}$ and RH-rd0>1 (i.e. RH of the wet months during which plant grow) is the closest to the one obtained between ^{17}O-excess$_{phyto}$ and RH in the growth chambers (fig. 4b). It can be expressed as follows (Eq.3):

$$^{17}\text{O-excess}_{phyto} = 3.4 \times (\text{RH-rd0>1}) - 460 \qquad (r^2 = 0.48;\ p < 0.001) \qquad \text{Eq. 1}$$

where ^{17}O-excess$_{phyto}$ is expressed in per meg and RH in %.

The excluded outliers (Table 3) are RIM1 and C3L4. RIM1 presents a very low ^{17}O-excess (-305 per meg) relative to the ^{17}O-excess of the samples with close RH-rd0>1, i.e. from 71 to 74 % (average of -237 ± 32 per meg for 82-78, 83-116 and 83-115). C3L4 is located next to C4L3 and under similar averaged RH but presents a ^{17}O-excess higher by 133 per meg. RIM1 and C3L4 show morphological patterns very similar to the other assemblages with the same range of RH. Thus, the discrepancies may lie either in the fact that local RH variations may not be reflected in RH averaged estimates for 10' (≈ 185 km^2) or in the particularity of the isotope composition of the local soil water (see discussion below).

The phytolith index d/p ranges from 0.01 to 0.08 in savanna, from 0.14 to 0.49 in wooded savanna, from 0.76 to 1.58 in enclosed savanna and from 1.84 to 6.78 in humid forests (Table 2). This unambiguous increase of d/p with tree cover density is in agreement with previous calibrations performed for the West African area (Bremond et al., 2005b). Interestingly, under high RH conditions, humid forest and enclosed savanna that are characterized by a large range of d/p represent a small range of ^{17}O-excess. Conversely, under lower RH conditions, savanna and wooded savanna that are characterized by a small range of d/p represent a large range of ^{17}O-excess (fig.5). This absence of relationship between ^{17}O-excess and tree cover density is also mirrored in figure 4 where phytolith samples from different vegetation types (i.e. savanna *vs* wooded savanna or humid forests *vs* enclosed savanna), that have developed under the same RH conditions, have the same range of ^{17}O-excess.

4 Discussion

4.1 Imprint of changes in atmospheric RH on the ^{17}O-excess of leaf water

In the bulk leaf water, the trends observed between $\Delta'^{18}O_{LW\text{-}IW}$ or ^{17}O-excess$_{e\ LW\text{-}IW}$ and RH are in agreement with an evaporative kinetic fractionation that increases when RH decreases, as expected from previous studies on the δ^{18}O or ^{17}O-excess evolution of leaf water (e.g. Cernusak et al., 2016; Landais et al., 2006; Li et al., 2017). The average value of $\lambda_{LW\text{-}IW}$ (0.519) is close to the value of θ_{diff} calculated for the diffusion of vapor in air (0.518; Barkan and Luz, 2007). As schematically described in Landais et al. (2016), λ_{transp} (equivalent to $\lambda_{LW\text{-}IW}$) represents the interplay among three processes in the leaf boundary layer: 1) the equilibrium fractionation, which is only temperature-dependent (Majoube, 1971) and drives the isotope composition of leaf water along the equilibrium water line ($\theta_{equil} = 0.529$); 2) the diffusion transport leading to increasing kinetic fractionation with decreasing relative humidity along the diffusion line; 3) the isotope exchange of leaf water with atmospheric water vapor, decreasing from turbulent to laminar and molecular leaf boundary layer vapor transport conditions (e.g. Buhay et al., 1996). In the case of the growth chamber experiment, the fact that $\lambda_{LW\text{-}IW}$ is close to θ_{diff} supports that the increasing diffusion of vapor in air when RH decreases or transpiration increases is the main process controling the evolution of ^{17}O-excess$_{LW}$. At high humidity (80-100% RH), the kinetic fractionation likely reaches its minimum as the diffusion process becomes limited.

The $\delta^{18}O_{LW}$ is commonly modelled as a function of the isotope composition of absorbed water, the isotope composition of water vapor, and RH (Craig and Gordon, 1965). The Craig and Gordon simple approach overestimates $\delta^{18}O_{LW}$ and different corrections have been proposed to take into account the diffusion of the evaporating water back to the leaf lamina and the advection of less evaporated stem water (i.e. the Péclet effect, Buhay et al., 1996; Helliker and Ehleringer, 2000; Roden et al., 2000; Farquhar and Gan, 2003; Farquhar and Cernusak, 2005; Ripullone et al., 2008; Treydte et al., 2014). In the growth chamber experiment, where water availability, relative humidity, and temperature were kept constant, we assume that transpiration rapidly reached a steady state and that the isotope composition of transpired water was the same as that of the irrigation water entering the plant (e.g. Welp et al., 2008). A tentative estimate of the theoretical value of $\Delta'^{18}O_{LW\text{-}IW}$, $\Delta'^{17}O_{LW\text{-}IW}$ and ^{17}O-excess$_{e\ LW\text{-}IW}$ was performed using the equations proposed for ^{18}O-enrichment by Cernusak et al. (2016) (table S3). For calculating the $\Delta^{17}{}_{LW\text{-}IW}$ we used for the equilibrium and kinetic fractionations (respectively $^{17}\alpha_{eq}$ and $^{17}\alpha_{k}$ in table S3) $^{17}\alpha_{eq} = {}^{18}\alpha_{eq}{}^{0.529}$ and $^{17}\alpha_{k} = {}^{18}\alpha_{k}{}^{0.518}$. As expected, the predicted $\Delta'^{18}O_{LW\text{-}IW}$ values were all higher than the observed values by several ‰. Helliker and Ehleringer (2000) proposed, for monocotyledonous species characterized by a vertical parallel veinal structure, to use instead of the Craig and Gordon model the Gat and Bowser (1991) equation describing the movement of water through a sequence of pools in series. However this model would further increase the estimates of $\Delta'^{18}O_{LW\text{-}IW}$. The predicted ^{17}O-excess$_{e}$ displayed in Table S3 was either higher or lower than the observed ^{17}O-excess$_{e\ LW\text{-}IW}$. Predicted $\lambda_{LW\text{-}IW}$ increased with RH from 0.521 to 0.529 which is far from the observed values averaging 0.519. The predicted value of 0.529 at 100 % RH reflects pure equilibrium in a situation where irrigation water and water vapor are assumed to have similar isotope composition since irrigation water is directly vaporized into the chamber (table S3), without any fractionation. Sensitivity tests show that regardless of the model chosen (Buhay et al., 1996; Cernusak et al., 2016; Li et al., 2017), estimations of $\lambda_{LW\text{-}IW}$ are very dependant on the isotope compositions of the water vapor (Li et al., 2017), not measured either in our experiment or in previous studies (Landais et al., 2006; Li et al., 2017). In the natural environment, a first order approximation for the isotope composition of water vapor is to consider equilibrium with precipitation. As a result of water-vapor equilibrium fractionation and soil water ^{18}O-enrichment, this can lead to a water vapor ^{18}O-depleted by 10-13 ‰ compared to the soil water (Landais et al., 2006; Lehmann et al., 2018). In this case the predicted λ_{transp} (equivalent to $\lambda_{LW\text{-}SW}$) decreases with increasing humidity. Finally, because wrong values of the isotope compositions of the water vapor may affect significantly the calculation of $\Delta'^{18}O_{LW\text{-}IW}$, Δ'^{17}O-excess$_{e\ LW\text{-}IW}$ and $\lambda_{LW\text{-}SW}$, we call for vapor isotope measurements as a prerequisite to accurately model the leaf water triple oxygen isotope evolution with RH. However, overall, despite the uncertainties on the predicted evolution of $\lambda_{LW\text{-}SW}$ with RH, the predicted value of ^{17}O-excess$_{e\ LW\text{-}IW}$ decreases when RH increases, which is also observed, as well as reflected in the triple isotope composition of phytoliths, as discussed below.

4.2 Imprint of changes in atmospheric RH on the ^{17}O-excess of phytoliths

Polymerization of silica is supposed to occur in isotope equilibrium with the forming-water, and therefore, to be only governed by temperature and the isotope composition of the forming water. Almost a dozen temperature-dependant relationships have been empirically established between the $\delta^{18}O$ of quartz, sinters, cherts, diatoms or phytoliths and the $\delta^{18}O$ of their forming water ($\delta^{18}O_{PhytoFW}$). Although the obtained fractionation coefficients are close (from -0.2 to -0.4 ‰ °C^{-1}), the range of fractionation ($\Delta^{18}O_{Phyto\text{-}PhytoFW}$) is large (see synthesis in Alexandre et al., 2012). The $\Delta^{18}O_{Phyto\text{-}LW}$ values obtained in the frame of the growth chamber experiment (ranging from 27.9 ± 7.2 to 32.3 ± 2.2‰) encompass the $\Delta^{18}O_{Phyto\text{-}PhytoFW}$ of 31.1‰ calculated from the Dodd and Sharp (2010) relationship for 25°C. It is lower than the values of 36.4 and 36 ‰ at 25 °C, calculated from Sharp et al. (2016) and Alexandre et al. (2012). Whereas Alexandre et al. (2012) and Sharp et al. (2016) generally estimated the forming-water $\delta^{18}O$ values, Dodd and Sharp (2010) measured the the $\delta^{18}O$ values of the water samples. The proximity of the obtained range of $\Delta^{18}O_{Phyto\text{-}LW}$ values to the $\Delta^{18}O_{Phyto\text{-}Phyto\ FW}$ calculated from Dodd and Sharp (2010) suggests that phytoliths formed in equilibrium with a water of isotope composition close to that of the bulk leaf water. This is additionally supported by the obtained averaged value of $\lambda_{Phyto\text{-}LW}$ (0.522 ± 0.001) close to the $\theta_{SiO2\text{-}water}$ equilibrium value of 0.524 calculated for 25 °C from Sharp et al. (2016).

Evolution of the triple isotope composition of bulk leaf water and phytoliths can be illustrated by plotting $\delta'^{17}O$ *vs* $\delta'^{18}O$, or ^{17}O-excess *vs* $\delta'^{18}O$ (fig. 6) which is more appropriate to evidence small variations. Figure 6 shows that the leaf water evolved from the irrigation water pool, becomes increasingly subject to kinetic fractionation when RH decreased. This evolution follows a single leaf water line reflecting $\lambda_{LW\text{-}IW} = 0.519$ (Table1). Then, if phytoliths polymerized from the bulk leaf waters, at 25°C, according to a constant equilibrium fractionation, their expected isotope signature should follow a line parallel to the leaf water line. This is the case for phytoliths formed at RH higher than 40%. However, the isotope signature of phytoliths formed at 40% RH suggest a forming water more evaporated than the bulk leaf water. The Péclet effect, which is known to scale with transpiration (e.g. Barnard et al., 2007) can explain this discrepancy. Advection of less evaporated stem water may decrease $\delta'^{18}O_{LW}$ and increase ^{17}O-excess$_{LW}$ relative to $\delta'^{18}O$ and ^{17}O-excess of the epidermal water prone to evaporation and from which phytoliths formed. At this point, the data scattering prevents further discussion but the possibility that when RH is low, or when transpiration is high, the phytolith forming-water is different from the bulk leaf water must be investigated in future research developments.

With regard to the natural samples, whereas no relationship was found between $\delta'^{18}O_{phyto}$ and RH, a clear positive linear dependency of ^{17}O-excess$_{phyto}$ to RH was shown, equivalent to 2.1 per meg / % when the annual RH average was taken into account, or to 3.4 per meg / % when the average of the growing season (RH-rd0>1) was taken into account (fig. 4). These coefficients are close to the slope of the lines obtained for the growth chamber experiment between ^{17}O-excess$_{Phyto}$, ^{17}O-excess$_{e\ LW\text{-}IW}$ and ^{17}O-excess$_{e\ Phyto\text{-}IW}$ and 80 to 40% RH (fig. 1a, e and f). This consistency represents a major positive step in examining whether changes in atmospheric RH imprint the ^{17}O-excess of natural phytolith assemblages in a predictable way. Without taking into account the two outliers, the linear regression between RH-rd0>1 and ^{17}O-excess$_{phyto}$ for a 95% confidence interval can be expressed as follows:

$$\text{RH-rd0>1} = 0.14 \pm 0.02 \text{ (S.E) x } ^{17}\text{O-excess}_{phyto} + 100.5 \pm 4.7 \text{ (S.E)} \qquad \text{Eq. 2}$$

where ^{17}O-excess$_{phyto}$ is expressed in per meg and RH in %, $r^2 = 0.48$, and $p < 0.001$. S.E. stands for standard error. The S.E. of the predicted RH-rd0>1value is ± 5.6%. However, the data scattering (fig. 4) call for assessing additional parameters that can contribute to changes in ^{17}O-excess$_{Phyto}$, beside RH, before using the ^{17}O-excess$_{phyto}$ for quantitative RH reconstruction.

One can expect that the isotope composition of the soil water taken-up by the roots impacts ^{17}O-excess$_{Phyto}$. In tropical dry and humid areas, evaporative kinetic fractionation can lead to a ^{18}O-enrichment of the soil water of several ‰, in the first dm depth (e.g. Gaj et al., 2016; Liu et al., 2010). Spatial variability in the composition of the rainfall feeding the upper soil water may also intervene. However, the amount-weighted values of $\delta'^{18}O_{Pre}$ along the sampled transect vary little (Table 2). With regard to ^{17}O-excess, changes in soil water evaporation rather than the small variations expected for ^{17}O-excess$_{Pre}$ (Landais et al., 2010b; Li et al., 2015) should impact the evolution of ^{17}O-excess$_{Phyto}$, although, here, the lack of measurements only allow for speculation.

The vegetation type and the plant part from which phytoliths come from may also bring some noise to the relationship between ^{17}O-excess$_{phyto}$ and RH. In grasses, leaf water is expected to be more prone to evaporative enrichment than stem water, and inside the leaf itself, the heterogeneity of evaporative sites repartition and water movements can lead to a significant heterogeneity in the $\delta^{18}O$ signatures of water and phytoliths (Cernusak et al., 2016; Helliker and Ehleringer, 2000; Webb and Longstaffe, 2002). However, soil top phytolith assemblages likely record several decades of annual bulk phytolith production and their isotope composition is expected to be an average. This would explain the consistency of the ^{17}O-excess$_{Phyto}$ data obtained from bulk grass phytoliths from climate chambers and the bulk phytolith assemblages from natural vegetation. Further investigation on the extent of the heterogeneity of ^{17}O-excess in water and phytoliths in mature grasses would help to verify this assumption. In trees, the Globular granulate phytolith is assumed to come from the non-transpiring secondary xylem of the wood. Thus Globular granulate phytoliths should present an isotope signature closer to that of the soil water, or less impacted by kinetic fractionation than grass phytoliths. However, for a given range of RH, samples with significant representations of both phytolith categories (i.e wooded savanna and enclosed savanna samples with d/p from 0.1 to 1.6) present ^{17}O-excess values close to the values obtained by samples with very low or very high d/p (figs. 4 and 5). To further assess the significance of the Globular granulate isotope signature, we calculated $\delta'^{18}O_{PhytoFW}$ values (Table 2) using the Dodd and Sharp (2010) fractionation factor and compared it to the precipitation-weighted $\delta'^{18}O_{Pre\text{-}rd0>1}$ average. For the humid forest assemblages, $\delta'^{18}O_{PhytoFW}$ values are higher than $\delta'^{18}O_{pre\ rd0>1}$ by 4.6 ± 1.5 ‰. This difference is larger than the range of ^{18}O-enrichment observed for the upper 10 cm depth of soil water under tropical humid forests (2-3‰; Liu et al., 2008; Stahl et al., 2013), suggesting that evaporative isotope signatures of both soils and leaf water imprinted the Globular granulate phytolith type. This is in line with recent ^{18}O-labelling experiment showing that the ^{18}O-enriched oak phloem water may exchange with xylem water under low transpiration rates (Lehmann et al., 2018). Complementary examination of the isotope signature of phytolith assemblages from forests growing under different RH conditions (i.e dry forests, humid forests, rainforests), as well as further investigation of the anatomical origin of the Globular granulate phytolith type are now required to further discuss the meaning of the ^{17}O-excess signal brought by wooded savanna and tropical forest phytolith assemblages.

Biases due to the calibration methodology may also be responsible for the data scattering. Imperfect adequacy between the space scales recorded by the soil top phytolith assemblages and the RH variables may come into play. Phytolith assemblages represent a mixture of local and wind-transported phytoliths. In the open saharian, sahelian and soudanian zones of West Africa the winter low altitude north-easterly trade winds may transport phytoliths southward, reducing differences between assemblages from different biogeographic zones and increasing differences among assemblages of a given biogeographic zone (Bremond et al., 2005b). Additional samples from other geographic zones are thus needed to increase the robustness of the relationship. With regard to the recorded time scales, the CRU RH 30 years averages are in agreement with the several decades of phytolith production.

5 Conclusion

The present combination of growth chamber and i*n situ* transect calibrations lay the groundwork for further examination of the robustness of the ^{17}O-excess$_{\mathrm{Phyto}}$ as a proxy of changes in RH. The growth chamber experiment demonstrated that change in RH imprints ^{17}O-excess$_{\mathrm{Phyto}}$ (by 4.1 per meg / % between 40 and 80% RH) or the ^{17}O-excess$_{\mathrm{e\ Phyto\text{-}IW}}$ (by 4.3 per meg / %, between 40 and 80% RH) through its imprint on ^{17}O-excess$_{\mathrm{e\ LW\text{-}IW}}$. As the isotope composition of the irrigation water was stable, and transpiration likely reached a steady state, the positive correlation between ^{17}O-excess$_{\mathrm{LW}}$ and RH was only governed by the kinetic fractionation occurring in the leaf epidermis water subject to evaporation, as supported by the averaged value of $\lambda_{\mathrm{LW\text{-}IW}}$ of 0.519, close to θ_{diff}.

In order to model the triple oxygen isotope fractionation in play at the soil/plant/atmosphere interface we require direct and continuous measurements of the triple isotope composition of water vapor. Such measurements should develop in the near futur through the use of isotope ratio infrared analyzers (e.g. Berkelhammer et al., 2013; Schmidt et al., 2010). We also suggest to constrain as much as possible the isotope composition of the soil water taken up by the roots. Stem water is usually used as an analogue of soil water when modelling $\delta'^{17}O_{\mathrm{LW}}$ and $\delta'^{18}O_{\mathrm{LW}}$ (Landais et al., 2006; Li et al., 2017). However, in the stem, water in the phloem that is bidirectional (moves up and down the plant's stem) receives the contribution of evaporating leaf water, and water in the xylem that is unidirectional (moves up the plant's stem) may exchange with phloem waters (Lehmann et al., 2018). Consequently one may expect the isotope composition of stem water to be slightly different than that of soil water (Berkelhammer et al., 2013; Treydte et al., 2014).

When plotting ^{17}O-excess$_{\mathrm{Phyto}}$ *vs* RH, the samples collected along the West and Central African relative humidity transect define a correlation coefficient ranging from 2.1 to 3.4 per meg / % (depending on the RH variable taken into account) and lay close to the growth chamber ^{17}O-excess$_{\mathrm{Phyto}}$ line. This supports that RH is an important control of ^{17}O-excess$_{\mathrm{Phyto}}$ in natural environment, even if phytolith assemblages come from different vegetation types. However, other parameters such as changes in the triple isotope composition of the soil water, vegetation source or imperfect adequation between the space scales recorded by the soil top phytolith assemblages and the RH variables may come into play and explain the scattering of ^{17}O-excess$_{\mathrm{Phyto}}$. Assessment of these parameters through additional growth chambers experiments and field campaigns will bring us closer to an accurate proxy of changes in relative humidity.

Acknowledgements

This study was supported by the French program INSU-LEFE and benefited from the CNRS human and technical resources allocated to the ECOTRONS Research Infrastructures as well as from the state allocation 'Investissements d'Avenir' ANR-11-INBS-0001.

References

Affolter, S., Häuselmann, A.D., Fleitmann, D., Häuselmann, P., and Leuenberger, M. (2015). Triple isotope (δD, δ17O, δ18O) study on precipitation, drip water and speleothem fluid inclusions for a Western Central European cave (NW Switzerland). Quat. Sci. Rev. *127*, 73–89.

Alexandre, A., and Brémond, L. (2009). Comment on the paper in Quaternary International: "Methodological concerns for analysis of phytolith assemblages: Does count size matter?" (C.A.E. Strömberg). Quat. Int. *193*, 141–142.

Alexandre, A., Meunier, J.-D., Colin, F., and Koud, J.-M. (1997). Plant impact on the biogeochemical cycle of silicon and related weathering processes. Geochim. Cosmochim. Acta *61*, 677–682.

Alexandre, A., Crespin, J., Sylvestre, F., Sonzogni, C., and Hilbert, D.W. (2012). The oxygen isotopic composition of phytolith assemblages from tropical rainforest soil tops (Queensland, Australia): validation of a new paleoenvironmental tool. Clim. Past *8*, 307–324.

Alexandre, A., Balesdent, J., Cazevieille, P., Chevassus-Rosset, C., Signoret, P., Mazur, J.-C., Harutyunyan, A., Doelsch, E., Basile-Doelsch, I., Miche, H., et al. (2016). Direct uptake of organically derived carbon by grass roots and allocation in leaves and phytoliths: 13C labeling evidence. Biogeosciences *13*, 1693–1703.

Alexandre, A.E., Pailles, C., Sonzogni, C., Kershaw, P., Wust, R.A., and Turney, C.S. (2013). δ^{18}O signature of phytoliths from the last interglacial Lynch's Crater sediments (Qld, Australia): insights on changes in precipitation sources. AGU Fall Meet. Abstr. *33*.

Andrade, J.M., and Estévez-Pérez, M.G. (2014). Statistical comparison of the slopes of two regression lines: A tutorial. Anal. Chim. Acta *838*, 1–12.

Angert, A., Rachmilevitch, S., Barkan, E., and Luz, B. (2003). Effects of photorespiration, the cytochrome pathway, and the alternative pathway on the triple isotopic composition of atmospheric O2. Glob. Biogeochem. Cycles *17*, 1030.

Angert, A., Cappa, C.D., and DePaolo, D.J. (2004). Kinetic O-17 effects in the hydrologic cycle:

Indirect evidence and implications. Geochim. Cosmochim. Acta *68*, 3487–3495.

Backwell, L.R., McCarthy, T.S., Wadley, L., Henderson, Z., Steininger, C.M., Bonita deKlerk, Barré, M., Lamothe, M., Chase, B.M., Woodborne, S., et al. (2014). Multiproxy record of late Quaternary climate change and Middle Stone Age human occupation at Wonderkrater, South Africa. Quat. Sci. Rev. *99*, 42–59.

Barkan, E., and Luz, B. (2005). High precision measurements of 17O/16O and 18O/16O ratios in H2O. Rapid Commun. Mass Spectrom. *19*, 3737–3742.

Barkan, E., and Luz, B. (2007). Diffusivity fractionations of H2(16)O/H2(17)O and H2(16)O/H2(18)O in air and their implications for isotope hydrology. Rapid Commun. Mass Spectrom. RCM *21*, 2999–3005.

Barnard, R.L., Salmon, Y., Kodama, N., Sörgel, K., Holst, J., Rennenberg, H., Gessler, A., and Buchmann, N. (2007). Evaporative enrichment and time lags between delta18O of leaf water and organic pools in a pine stand. Plant Cell Environ. *30*, 539–550.

Bartlein, P.J., Harrison, S.P., Brewer, S., Connor, S., Davis, B. a. S., Gajewski, K., Guiot, J., Harrison-Prentice, T.I., Henderson, A., Peyron, O., et al. (2010). Pollen-based continental climate reconstructions at 6 and 21 ka: a global synthesis. Clim. Dyn. *37*, 775–802.

Berkelhammer, M., Hu, J., Bailey, A., Noone, D.C., Still, C.J., Barnard, H., Gochis, D., Hsiao, G.S., Rahn, T., and Turnipseed, A. (2013). The nocturnal water cycle in an open-canopy forest. J. Geophys. Res. Atmospheres *118*, 10,225-10,242.

Bony, S., Colman, R., Kattsov, V.M., Allan, R.P., Bretherton, C.S., Dufresne, J.L., Hall, A., Hallegatte, S., Holland, M.M., Ingram, W., et al. (2006). How well do we understand and evaluate climate change feedback processes? J. Clim. *19*, 3445–3482.

Bowen, G.J., and Revenaugh, J. (2003). Interpolating the isotopic composition of modern meteoric precipitation. Water Resour. Res. *39*, 1299.

Bowen, G.J., and Wilkinson, B. (2002). Spatial distribution of δ18O in meteoric precipitation. Geology *30*, 315–318.

Bowen, G.J., Wassenaar, L.I., and Hobson, K.A. (2005). Global application of stable hydrogen and oxygen isotopes to wildlife forensics. Oecologia *143*, 337–348.

Bowling, D.R., Schulze, E.S., and Hall, S.J. (2017). Revisiting streamside trees that do not use stream water: can the two water worlds hypothesis and snowpack isotopic effects explain a missing water source? Ecohydrology *10*, n/a-n/a.

Bremond, L., Alexandre, A., Hely, C., and Guiot, J. (2005a). A phytolith index as a proxy of tree cover density in tropical areas: Calibration with Leaf Area Index along a forest-savanna transect in southeastern Cameroon. Glob. Planet. Change *45*, 277–293.

Bremond, L., Alexandre, A., Peyron, O., and Guiot, J. (2005b). Grass water stress estimated from phytoliths in West Africa. J. Biogeogr. *32*, 311–327.

Bremond, L., Alexandre, A., Peyron, O., and Guiot, J. (2005c). Grass water stress estimated from phytoliths in West Africa. J. Biogeogr. *32*, 311–327.

Buhay, W.M., Edwards, T.W.D., and Aravena, R. (1996). Evaluating kinetic fractionation factors used for reconstructions from oxgen and hydrogen isotope ratios in plant water and cellulose. Geochim. Cosmochim. Acta *60*, 2209–2218.

Cernusak, L.A., Barbour, M.M., Arndt, S.K., Cheesman, A.W., English, N.B., Feild, T.S., Helliker, B.R., Holloway-Phillips, M.M., Holtum, J.A.M., Kahmen, A., et al. (2016). Stable isotopes in leaf water of terrestrial plants. Plant Cell Environ. *39*, 1087–1102.

Chapligin, B., Leng, M.J., Webb, E., Alexandre, A., Dodd, J.P., Ijiri, A., Lücke, A., Shemesh, A., Abelmann, A., Herzschuh, U., et al. (2011). Inter-laboratory comparison of oxygen isotope compositions from biogenic silica. Geochim. Cosmochim. Acta *75*, 7242–7256.

Chen, G., Auerswald, K., and Schnyder, H. (2016). 2H and 18O depletion of water close to organic surfaces. Biogeosciences *13*, 3175–3186.

Chung, E.-S., Soden, B., Sohn, B.J., and Shi, L. (2014). Upper-tropospheric moistening in response to anthropogenic warming. Proc. Natl. Acad. Sci. *111*, 11636–11641.

Collura, L.V., and Neumann, K. (2017). Wood and bark phytoliths of West African woody plants. Quat. Int. *434*, *Part B*, 142–159.

Contreras, D.A., Robin, V., Gonda, R., Hodara, R., Dal Corso, M., and Makarewicz, C. (2014). (Before and) After the Flood: A multiproxy approach to past floodplain usage in the middle Wadi el-Hasa, Jordan. J. Arid Environ. *110*, 30–43.

Crespin, J., Alexandre, A., Sylvestre, F., Sonzogni, C., Paillès, C., and Garreta, V. (2008). IR laser extraction technique applied to oxygen isotope analysis of small biogenic silica samples. Anal. Chem. *80*, 2372–2378.

Delattre, H., Vallet-Coulomb, C., and Sonzogni, C. (2015). Deuterium excess in atmospheric water vapor of a Mediterranean coastal wetland: regional versus local signatures. Atmos Chem Phys Discuss *15*, 1703–1746.

Dessler, A.E., and Davis, S.M. (2010). Trends in tropospheric humidity from reanalysis systems. J. Geophys. Res. Atmospheres *115*, D19127.

Dodd, J.P., and Sharp, Z.D. (2010). A laser fluorination method for oxygen isotope analysis of biogenic silica and a new oxygen isotope calibration of modern diatoms in freshwater environments. Geochim. Cosmochim. Acta *74*, 1381–1390.

Evaristo, J., Jasechko, S., and McDonnell, J.J. (2015). Global separation of plant transpiration from groundwater and streamflow. Nature *525*, 91–94.

Farquhar, G.D., and Cernusak, L.A. (2005). On the isotopic composition of leaf water in the non-steady state. Funct. Plant Biol. *32*, 293–303.

Farquhar, G.D., and Gan, K.S. (2003). On the progressive enrichment of the oxygen isotopic composition of water along a leaf. Plant Cell Environ. *26*, 801–819.

Fischer, E.M., and Knutti, R. (2013). Robust projections of combined humidity and temperature extremes. Nat. Clim. Change *3*, 126–130.

Gaj, M., Beyer, M., Koeniger, P., Wanke, H., Hamutoko, J., and Himmelsbach, T. (2016). In situ unsaturated zone water stable isotope (2 H and 18 O) measurements in semi-arid environments: a soil water balance. Hydrol. Earth Syst. Sci. *20*, 715–731.

Gat, J., and Bowser, C. (1991). Stable Isotope Geochemistry: A Tribute to Samuel Epstein (The Geochemical Society Special Publication No. 3).

Gázquez, F., Mather, I., Rolfe, J., Evans, N.P., Herwartz, D., Staubwasser, M., and Hodell, D.A. (2015). Simultaneous analysis of 17O/16O, 18O/16O and 2H/1H of gypsum hydration water by cavity ring-down laser spectroscopy. Rapid Commun. Mass Spectrom. *29*, 1997–2006.

Grießinger, J., Bräuning, A., Helle, G., Hochreuther, P., and Schleser, G. (2016). Late Holocene relative humidity history on the southeastern Tibetan plateau inferred from a tree-ring δ18O record: Recent decrease and conditions during the last 1500 years. Quat. Int.

Guillevic, M., Bazin, L., Landais, A., Stowasser, C., Masson-Delmotte, V., Blunier, T., Eynaud, F., Falourd, S., Michel, E., Minster, B., et al. (2014). Evidence for a three-phase sequence during Heinrich Stadial 4 using a multiproxy approach based on Greenland ice core records. Clim Past *10*, 2115–2133.

Held, I.M., and Soden, B.J. (2000). Water Vapor Feedback and Global Warming1. Annu. Rev. Energy Environ. *25*, 441–475.

Helliker, B.R., and Ehleringer, J.R. (2000). Establishing a grassland signature in veins: 18O in the leaf water of C3 and C4 grasses. Proc. Natl. Acad. Sci. U. S. A. *97*, 7894–7898.

Herbert, A.V., and Harrison, S.P. (2016). Evaluation of a modern-analogue methodology for reconstructing Australian palaeoclimate from pollen. Rev. Palaeobot. Palynol. *226*, 65–77.

Herwartz, D., Pack, A., Krylov, D., Xiao, Y., Muehlenbachs, K., Sengupta, S., and Rocco, T.D. Proceedings of the National Academy of Sciences.

IAEA (2013). A Laboratory Information Management System for Stable Hydrogen and Oxygen Isotopes in Water Samples by Laser Absorption Spectroscopy. User Manual & Tutorial.

Kriticos, D.J., Webber, B.L., Leriche, A., Ota, N., Macadam, I., Bathols, J., and Scott, J.K. (2012). CliMond: global high-resolution historical and future scenario climate surfaces for bioclimatic modelling. Methods Ecol. Evol. *3*, 53–64.

Kumar, S., Milstein, Y., Brami, Y., Elbaum, M., and Elbaum, R. (2017). Mechanism of silica deposition in sorghum silica cells. New Phytol. *213*, 791–798.

Labuhn, I., Daux, V., Girardclos, O., Stievenard, M., Pierre, M., and Masson-Delmotte, V. (2015). French summer droughts since 1326 AD: a reconstruction based on tree ring cellulose δ18O. Clim Past Discuss *11*, 5113–5155.

Labuhn, I., Daux, V., Girardclos, O., Stievenard, M., Pierre, M., and Masson-Delmotte, V. (2016). French summer droughts since 1326 CE: a reconstruction based on tree ring cellulose δ18O. Clim Past *12*, 1101–1117.

Landais, A., Barkan, E., Yakir, D., and Luz, B. (2006). The triple isotopic composition of oxygen in leaf water. Geochim. Cosmochim. Acta *70*, 4105–4115.

Landais, A., Barkan, E., and Luz, B. (2008). Record of δ18O and 17O-excess in ice from Vostok Antarctica during the last 150,000 years. Geophys. Res. Lett. *35*, L02709.

Landais, A., Dreyfus, G., Capron, E., Masson-Delmotte, V., Sanchez-Goñi, M.F., Desprat, S., Hoffmann, G., Jouzel, J., Leuenberger, M., and Johnsen, S. (2010a). What drives the millennial and orbital variations of δ18Oatm? Quat. Sci. Rev. *29*, 235–246.

Landais, A., Risi, C., Bony, S., Vimeux, F., Descroix, L., Falourd, S., and Bouygues, A. (2010b). Combined measurements of 17Oexcess and d-excess in African monsoon precipitation: Implications for evaluating convective parameterizations. Earth Planet. Sci. Lett. *298*, 104–112.

Lavergne, A., Daux, V., Villalba, R., Pierre, M., Stievenard, M., and Srur, A.M. (2017). Improvement of isotope-based climate reconstructions in Patagonia through a better understanding of climate influences on isotopic fractionation in tree rings. Earth Planet. Sci. Lett. *459*, 372–380.

Lezine, A.M. (1988). New pollen data from the Sahel, Senegal. In Review of Palaeobotany and Palynology, (Elsevier), pp. 141–154.

Li, S., Levin, N.E., and Chesson, L.A. (2015). Continental scale variation in 17O-excess of meteoric waters in the United States. Geochim. Cosmochim. Acta *164*, 110–126.

Li, S., Levin, N.E., Soderberg, K., Dennis, K.J., and Caylor, K.K. (2017). Triple oxygen isotope composition of leaf waters in Mpala, central Kenya. Earth Planet. Sci. Lett. *468*, 38–50.

Liu, W., Liu, W., Li, P., Duan, W., and Li, H. (2010). Dry season water uptake by two dominant canopy tree species in a tropical seasonal rainforest of Xishuangbanna, SW China. Agric. For. Meteorol. *150*, 380–388.

Liu, W.J., Liu, W.Y., Li, J.T., Wu, Z.W., and Li, H.M. (2008). Isotope variations of throughfall, stemflow and soil water in a tropical rain forest and a rubber plantation in Xishuangbanna, SW China. Hydrol. Res. *39*, 437–449.

Luz, B., and Barkan, E. (2010). Variations of 17O/16O and 18O/16O in meteoric waters.

Geochim. Cosmochim. Acta *74*, 6276–6286.

Ma, J.F., and Yamaji, N. (2006). Silicon uptake and accumulation in higher plants. Trends Plant Sci. *11*, 392–397.

Ma, J.F., Tamai, K., Yamaji, N., Mitani, N., Konishi, S., Katsuhara, M., Ishiguro, M., Murata, Y., and Yano, M. (2006). A silicon transporter in rice. Nature *440*, 688–691.

Madella, M., Alexandré, A., Ball, T., Group, I.W., and others (2005). International code for phytolith nomenclature 1.0. Ann. Bot. *96*, 253–260.

Majoube, M. (1971). Fractionnement en oxygène 18 et en deutérium entre l'eau et sa vapeur. J. Chim. Phys. *68*, 1423–1436.

Martín-Gómez, P., Barbeta, A., Voltas, J., Peñuelas, J., Dennis, K., Palacio, S., Dawson, T.E., and Ferrio, J.P. (2015). Isotope-ratio infrared spectroscopy: a reliable tool for the investigation of plant-water sources? New Phytol. *207*, 914–927.

Miller, M.F. (2002). Isotopic fractionation and the quantification of 17O anomalies in the oxygen three-isotope system: an appraisal and geochemical significance. Geochim. Cosmochim. Acta *66*, 1881–1889.

Miller, M.F., Greenwood, R.C., and Franchi, I.A. (2015). Comment on "The triple oxygen isotope composition of the Earth mantle and understanding Δ17O variations in terrestrial rocks and minerals" by Pack and Herwartz [Earth Planet. Sci. Lett. 390 (2014) 138–145]. ResearchGate *418*.

New, M., Lister, D., Hulme, M., and Makin, I. (2002). A high-resolution data set of surface climate over global land areas. Clim. Res. *21*, 1–25.

Oerter, E., Finstad, K., Schaefer, J., Goldsmith, G.R., Dawson, T., and Amundson, R. (2014). Oxygen isotope fractionation effects in soil water via interaction with cations (Mg, Ca, K, Na) adsorbed to phyllosilicate clay minerals. J. Hydrol. *515*, 1–9.

Orlowski, N., Pratt, D.L., and McDonnell, J.J. (2016). Intercomparison of soil pore water extraction methods for stable isotope analysis. Hydrol. Process. *30*, 3434–3449.

Pack, A., and Herwartz, D. (2014). The triple oxygen isotope composition of the Earth mantle and understanding variations in terrestrial rocks and minerals. Earth Planet. Sci. Lett. *390*, 138–145.

Passey, B.H., Hu, H., Ji, H., Montanari, S., Li, S., Henkes, G.A., and Levin, N.E. (2014). Triple oxygen isotopes in biogenic and sedimentary carbonates. Geochim. Cosmochim. Acta *141*, 1–25.

Piperno, D.R. (2006). Phytoliths: A Comprehensive Guide for Archaeologists and Paleoecologists (Rowman Altamira).

Ripullone, F., Matsuo, N., Stuart-Williams, H., Wong, S.C., Borghetti, M., Tani, M., and Farquhar, G. (2008). Environmental Effects on Oxygen Isotope Enrichment of Leaf Water in Cotton Leaves. Plant Physiol. *146*, 729–736.

Risi, C., Landais, A., Bony, S., Jouzel, J., Masson-Delmotte, V., and Vimeux, F. (2010). Understanding the 17O excess glacial-interglacial variations in Vostok precipitation. J. Geophys. Res. Atmospheres *115*, D10112.

Risi, C., Landais, A., Winkler, R., and Vimeux, F. (2013). Can we determine what controls the spatio-temporal distribution of d-excess and 17O-excess in precipitation using the LMDZ general circulation model? Clim Past *9*, 2173–2193.

Schmidt, M., Maseyk, K., Lett, C., Biron, P., Richard, P., Bariac, T., and Seibt, U. (2010). Concentration effects on laser-based δ18O and δ2H measurements and implications for the calibration of vapour measurements with liquid standards. Rapid Commun. Mass Spectrom. *24*, 3553–3561.

Schwab, V.F., Garcin, Y., Sachse, D., Todou, G., Séné, O., Onana, J.-M., Achoundong, G., and Gleixner, G. (2015). Effect of aridity on δ13C and δD values of C3 plant- and C4 graminoid-derived leaf wax lipids from soils along an environmental gradient in Cameroon (Western Central Africa). Org. Geochem. *78*, 99–109.

Scurfield, G., Anderson, and Segnit (1974). Silica in woody stems. Aust. J. Bot *22*, 211–229.

Sharp, Z.D., Gibbons, J.A., Maltsev, O., Atudorei, V., Pack, A., Sengupta, S., Shock, E.L., and Knauth, L.P. (2016). A calibration of the triple oxygen isotope fractionation in the SiO2–H2O system and applications to natural samples. Geochim. Cosmochim. Acta *186*, 105–119.

Sherwood, S.C., Ingram, W., Tsushima, Y., Satoh, M., Roberts, M., Vidale, P.L., and O'Gorman, P.A. (2010). Relative humidity changes in a warmer climate. J. Geophys. Res. Atmospheres *115*, D09104.

Stahl, C., Hérault, B., Rossi, V., Burban, B., Bréchet, C., and Bonal, D. (2013). Depth of soil water uptake by tropical rainforest trees during dry periods: does tree dimension matter? Oecologia *173*, 1191–1201.

Steig, E.J., Gkinis, V., Schauer, A.J., Schoenemann, S.W., Samek, K., Hoffnagle, J., Dennis, K.J., and Tan, S.M. (2014). Calibrated high-precision 17O-excess measurements using cavity ring-down spectroscopy with laser-current-tuned cavity resonance. Atmospheric Meas. Tech. *7*, 2421–2435.

Suavet, C., Alexandre, A., Franchi, I.A., Gattacceca, J., Sonzogni, C., Greenwood, R.C., Folco, L., and Rochette, P. (2010). Identification of the parent bodies of micrometeorites with high-precision oxygen isotope ratios. Earth Planet. Sci. Lett. *293*, 313–320.

Treydte, K., Boda, S., Graf Pannatier, E., Fonti, P., Frank, D., Ullrich, B., Saurer, M., Siegwolf, R., Battipaglia, G., Werner, W., et al. (2014). Seasonal transfer of oxygen isotopes from precipitation and soil to the tree ring: source water versus needle water enrichment. New Phytol. *202*, 772–783.

Tuthorn, M., Zech, R., Ruppenthal, M., Oelmann, Y., Kahmen, A., del Valle, H.F., Eglinton, T., Rozanski, K., and Zech, M. (2015). Coupling δ2H and δ18O biomarker results yields information on relative humidity and isotopic composition of precipitation – a climate transect validation study. Biogeosciences *12*, 3913–3924.

Uemura, R., Barkan, E., Abe, O., and Luz, B. (2010). Triple isotope composition of oxygen in atmospheric water vapor. Geophys. Res. Lett. *37*, L04402.

Valley, J.W., Kitchen, N., Kohn, M.J., Niendorf, C.R., and Spicuzza, M.J. (1995). UWG-2, a garnet standard for oxygen isotope ratios: Strategies for high precision and accuracy with laser heating. Geochim. Cosmochim. Acta *59*, 5223–5231.

Wahl, E.R., Diaz, H.F., and Ohlwein, C. (2012). A pollen-based reconstruction of summer temperature in central North America and implications for circulation patterns during medieval times. Glob. Planet. Change *84–85*, 66–74.

Webb, E.A., and Longstaffe, F.J. (2000). The oxygen isotopic compositions of silica phytoliths and plant water in grasses: Implications for the study of paleoclimate. Geochim. Cosmochim. Acta *64*, 767–780.

Webb, E.A., and Longstaffe, F.J. (2002). Climatic influences on the oxygen isotopic composition of biogenic silica in prairie grass. Geochim. Cosmochim. Acta *66*, 1891–1904.

Webb, E.A., and Longstaffe, F.J. (2003). The relationship between phytolith- and plant-water delta O-18 values in grasses. Geochim. Cosmochim. Acta *67*, 1437–1449.

Webb, E.A., and Longstaffe, F.J. (2006). Identifying the δ 18O signature of precipitation in grass cellulose and phytoliths: Refining the paleoclimate model. Geochim. Cosmochim. Acta *70*, 2417–2426.

Welle, B.J.H. ter (1976). On the occurrence of Silica grains in the secondary xylem of the Chrysobalanaceae.

Welp, L.R., Lee, X., Kim, K., Griffis, T.J., Billmark, K.A., and Baker, J.M. (2008). δ18O of water vapour, evapotranspiration and the sites of leaf water evaporation in a soybean canopy. Plant Cell Environ. *31*, 1214–1228.

Wernicke, J., Grießinger, J., Hochreuther, P., and Bräuning, A. (2015). Variability of summer humidity during the past 800 years on the eastern Tibetan Plateau inferred from δ18O of tree-ring cellulose. Clim Past *11*, 327–337.

White, F., Unesco, and Office, U.N.S.-S. (1983). The vegetation of Africa: a descriptive memoir to accompany the Unesco/AETFAT/UNSO vegetation map of Africa (Unesco).

Table 1. Growth chamber experiment : experimental set-up, phytolith content and morphological characteristics, isotope enrichments ($\Delta'^{*}_{A\text{-}B} = {}^{*}\delta'_{a} - {}^{*}\delta'_{b}$), associated ^{17}O-excess$_e$ (^{17}O-excess$_e$ = $\Delta'^{17} - 0.528 \times \Delta'^{18}$), λ ($\lambda = \Delta'^{17} / \Delta'^{18}$) of phytoliths compared to either leaf water or irrigation water and of leaf water compared to irrigation water. Av : average ; n : number of replicates ; SD : standard deviation calculated on the replicates; n.v. : no value. Transp. (l/day), Conc. (% d.w.) and LC (%) stands for transpiration expressed in liter/day, phytolith concentration expressed in % of the dry weight and long cell abundance in the phytolith morphological assemblage expressed in % of counted phytoliths with taxonomic significance, respectively. Samples are named according to the climate chamber # they were collected in (e.g. P1, P2), the set relative humidity (e.g. 40, 60) and the date of sampling (e.g. 29-04-16 for dd/mm/yy).

Experimental set-up								Phytoliths (Phyto)			Leaf water -irrigation water (LW-IW)				Phytolith - leaf water (Phyto-LW)				Phytolith -irrigation water (Phyto-IW)			
Duration	Temp.	SD	RH	SD	Light	Transp.	Biomass	Sample	Conc.	LC	$\Delta'^{18}O$	$\Delta'^{17}O$	^{17}O-excess$_e$	λ	$\Delta'^{18}O$	$\Delta'^{17}O$	^{17}O-excess$_e$	λ	$\Delta'^{18}O$	$\Delta'^{17}O$	^{17}O-excess$_e$	λ
day	°C		%		mmol/m^2/sec	l/day	g		% d.w.	%		‰	per meg			‰	per meg			‰	per meg	
11	25	0.2	41.2	1	278		13	P1-40-29-04-16	n.v.		16.238	8.420	-154	0.519	33.776	17.589	-244	0.521	50.013	26.009	-398	0.520
10	25	0.2	41.3	1.1	278	0.49	21	P10-40-10-05-16	0.8		13.171	6.799	-155	0.516	33.530	17.498	-206	0.522	46.701	24.297	-361	0.520
11	25	0.4	41.9	1	311	0.69	37	P1-40-20-05-16	0.8	21	16.345	8.460	-170	0.518	29.577	15.401	-216	0.521	45.922	23.861	-385	0.520
14	25	0.2	41.4	0.9	278	0.65	38	P1-40-03-06-16	1.8		n.v.	n.v.	n.v.	n.v.	32.415	16.874	-241	0.521	n.v.	n.v.	n.v.	n.v.
					Av.	**0.61**			**1.2**		**15.251**	**7.893**	**-159**	**0.517**	**32.324**	**16.840**	**-227**	**0.521**	**47.545**	**24.723**	**-381**	**0.520**
					SD	**0.11**			**0.6**		**1.802**	**0.947**	**9**	**0.001**	**1.925**	**1.011**	**19**	**0.0006**	**2.172**	**1.135**	**19**	**0.0003**
11	25	0.5	60.2	2.5	311		21	P10-60-29-04-16	n.v.		15.115	7.864	-117	0.520	29.133	15.211	-171	0.522	44.248	23.075	-288	0.521
11	25	0.2	60.5	1	289	0.57	33	P2-60-10-05-16	0.7		16.885	8.737	-178	0.517	25.877	13.575	-88	0.525	42.761	22.312	-266	0.522
10	25	0.8	60.2	4.8	311	0.60	48	P10-60-20-05-16	0.8	13	12.014	6.242	-101	0.520	30.254	15.804	-170	0.522	42.268	22.047	-271	0.522
14	25	0.6	60.3	3.2	311	0.76	60	P10-60-03-06-16	1.3		n.v.	n.v.	n.v.	n.v.	32.915	17.186	-193	0.522	n.v.	n.v.	n.v.	n.v.
					Av.	**0.64**			**0.9**		**14.671**	**7.614**	**-132**	**0.519**	**29.545**	**15.444**	**-156**	**0.523**	**43.093**	**22.478**	**-275**	**0.522**
					SD	**0.10**			**0.3**		**2.465**	**1.266**	**41**	**0.001**	**2.915**	**1.496**	**46**	**0.0012**	**1.031**	**0.534**	**11**	**0.0001**
11	25	0.2	80.2	2.8	289		24	P2-85-29-04-16	n.v.		7.826	4.067	-65	0.520	28.039	14.668	-136	0.523	35.865	18.736	-201	0.522
10	25	0.2	81.5	1.3	289	0.28	27	P1-85-10-05-16	0.4		7.957	4.139	-62	0.520	28.276	14.783	-147	0.523	36.233	18.922	-209	0.522
11	25	0.2	76.6	2.5	278	0.22	27	P2-85-20-05-16	0.6	10	6.679	3.429	-97	0.513	28.668	14.993	-144	0.523	35.347	18.422	-241	0.521
14	25	0.2	82.5	1.1	289	0.36	37	P2-85-03-06-16	1.0		n.v.	n.v.	n.v.	n.v.	28.888	15.041	-212	0.521	n.v.	n.v.	n.v.	n.v.
					Av.	**0.29**			**0.7**		**7.487**	**3.879**	**-75**	**0.518**	**28.468**	**14.871**	**-160**	**0.522**	**35.815**	**18.694**	**-217**	**0.522**
					SD	**0.07**			**0.3**		**0.703**	**0.391**	**20**	**0.004**	**0.382**	**0.176**	**35**	**0.0012**	**0.445**	**0.253**	**21**	**0.0007**
11	25		100.0		307	0.03	31	P3-100-10-05-16	0.0		14.681	7.630	-122	0.520	21.325	11.170	-90	0.524	36.006	18.800	-212	0.522
10	25		100.0		307	0.01		P3-100-20-05-16	0.0	5	7.706	4.014	-54	0.521	27.344	14.284	-153	0.522	35.050	18.299	-208	0.522
14	25		100.0		307	0.05	21	P3-100-03-06-16	0.2		n.v.	n.v.	n.v.	n.v.	35.233	18.403	-200	0.522	n.v.	n.v.	n.v.	n.v.
					Av.	**0.03**			**0.1**		**11.194**	**5.822**	**-88**	**0.520**	**27.968**	**14.619**	**-148**	**0.523**	**35.528**	**18.549**	**-210**	**0.522**
					SD	**0.02**			**0.1**		**4.932**	**2.557**	**48**	**0.001**	**6.975**	**3.628**	**55**	**0.0008**	**0.676**	**0.354**	**3**	**0.0000**
								Av.(a)						**0.519**				**0.522**				
								SD (a)						**0.002**				**0.001**				

(a) Calculated on the raw values

Table 2. Natural West and Central African phytolith samples: coordinates, climatic parameters, calculated phytolith index d/p, measured $\delta'^{18}O_{Phyto}$, $\delta'^{17}O_{Phyto}$, ^{17}O-excess$_{Phyto}$, calculated $\delta'^{18}O$ of phytolith forming water ($\delta^{18}O_{PhytoFW}$) and precipitation-weighted $\delta'^{18}O_{Pre\text{-}rd0>1}$. Average and standard deviation (SD) are given for replicates. MAP: Mean Annual Precipitation; MAT: Mean Annual Temperature; RH: mean annual relative humidity; RH15: RH at 15:00 H UTC; RH-rd0>1: relative humidity average for months with at least one day with precipitation higher than 0.1mm; RH15-rd0>1: RHrd0>1 at 15:00 H UTC. See text for data source and calculation.

Identifier	Lat	long	MAP	MAT	RH	RH-rd0>1	RH15	RH15-rd0>1	$\delta'^{18}O_{Pre}$ (1)	d/p	n	$\delta'^{18}O_{Phyto}$	SD	$\delta'^{17}O_{Phyto}$	SD	^{17}O-excess$_{Phyto}$	SD	$\delta'^{18}O_{Phyto\ FW}$	$\Delta'^{18}O_{Phyto\text{-}Pre\text{-}rd0>1}$
			mm	°C	%	%	%	%	‰			‰		‰		per meg		‰	
Savana																			
RIM 3	21.5	-13.0	52.4	27.3	47.1	61.7	35.4	47.0	-3.220	0.03		33.127		17.218		-243		2.384	36.351
RIM 8	21.0	-12.2	49.1	28.2	44.1	60.5	33.0	45.9	-3.420	0.04		34.813		18.304		-243		4.221	38.239
MAU06	20.6	-12.6	68.8	27.6	44.0	58.0	33.0	44.1	-3.829	0.04		28.871		15.088		-268		-1.816	32.707
RIM 11	16.9	-15.2	209.1	27.3	45.9	68.5	32.5	52.2	-4.047	0.04		37.506		19.785		-211		6.745	41.561
RIM 10	16.7	-15.2	227.6	27.2	45.7	68.7	32.1	52.1	-4.042	0.01		38.163		20.094		-256		7.377	42.214
S33	16.4	-14.8	270.5	27.7	42.7	57.6	29.7	41.8	-3.861	0.04		35.961		18.939		-225		5.276	39.829
S32	16.3	-15.4	284.4	27.3	46.9	61.6	33.5	46.2	-3.768	0.04		37.297		19.617		-266		6.537	41.072
C4L1	16.1	-14.0	287.7	29.8	40.9	57.1	29.4	42.9	-3.874	0.02	2	34.915	0.368	18.340	0.203	-262	11	4.609	38.797
S40	16.1	-13.9	329.1	29.2	40.6	56.8	29.4	43.0	-3.969	0.06		35.385		18.592		-262		4.967	39.363
S29	16.1	-14.9	313.0	27.8	43.6	59.1	30.8	43.7	-3.833	0.05	2	35.449	0.583	18.653	0.303	-236	0	4.785	39.290
82-46	16.0	-16.0	316.4	27.1	53.0	67.5	40.1	54.2	-3.604	0.03		33.575		17.654		-228		2.800	37.185
82-47	16.0	-16.0	316.4	27.1	53.0	67.5	40.1	54.2	-3.604	0.04		36.429		19.169		-247		5.642	40.039
S44	15.8	-13.5	369.1	29.6	40.2	57.2	29.6	44.1	-4.073	0.04	2	36.211	0.593	19.041	0.284	-258	24	5.863	40.292
C4L3	15.4	-13.7	467.7	29.6	41.2	59.1	30.3	45.7	-4.023	0.05	2	33.688	0.312	17.652	0.175	-290	13	3.345	37.719
S54	15.3	-13.0	443.6	29.7	41.3	60.0	31.0	47.2	-4.009	0.04		35.586		18.680		-282		5.261	39.603
S58	15.1	-12.8	478.6	29.7	42.0	56.3	31.7	44.3	-4.009	0.05	2	36.161	0.234	19.006	0.143	-266	21	5.833	40.179
C5L1	15.0	-12.9	583.2	29.7	42.5	57.2	32.1	44.9	-3.972	0.06	3	29.525	0.483	15.500	0.257	-208	7	-0.787	33.505
83-62	14.9	-12.3	515.8	29.7	42.9	58.1	32.6	46.0	-4.097	0.06	2	36.320	0.747	19.095	0.424	-262	36	5.987	40.426
S5	14.7	-16.2	511.1	28.1	53.3	68.6	39.2	53.9	-3.789	0.08	2	24.297	0.115	12.704	0.064	-205	4	-6.312	28.094
82-79	14.2	-16.1	669.0	28.3	54.2	70.1	39.9	55.2	-3.774	0.03	2	33.913	0.046	17.798	0.076	-229		3.356	37.694
83-75	14.1	-12.7	736.2	29.1	46.7	63.1	35.6	50.3	-3.936	0.03		32.418		16.969		-290		2.000	36.362
82-78	14.1	-16.1	669.0	28.3	55.2	71.0	40.8	56.2	-3.768	0.18		23.789		12.437		-201		-6.785	27.565
S84	13.9	-13.4	775.2	28.9	47.4	64.1	36.1	50.9	-4.040	0.03	2	32.600	0.435	17.080	0.221	-277	5	2.141	36.648
S118	13.6	-13.7	878.1	28.6	49.6	66.3	37.7	52.9	-4.008	0.02		30.007		15.779		-188		-0.501	34.023
S88	13.6	-13.6	880.0	28.6	49.4	66.2	37.7	52.9	-3.996	0.02		28.371		14.900		-189		-2.129	32.375
83-120	13.5	-13.8	934.5	28.5	50.7	67.3	38.7	53.8	-3.984	0.05		31.622		16.570		-262		1.101	35.614
83-122	13.4	-14.9	947.3	28.1	53.6	68.1	39.8	53.7	-3.928	0.03	2	31.240	0.628	16.396	0.335	-231	9	0.649	35.176
S122	13.3	-13.9	934.5	28.5	52.1	68.1	39.7	53.7	-3.971	0.03		34.379		18.095		-219		3.851	38.350
S93	13.3	-13.2	1005.3	28.6	51.6	68.2	39.7	55.1	-3.925	0.08		30.064		15.787		-211		-0.435	33.989
83-98	13.1	-12.8	1067.0	28.7	52.7	69.3	40.8	56.3	-4.060	0.04		29.692		15.621		-177		-0.800	33.753
S128	13.0	-14.1	1055.1	28.2	54.7	70.2	41.7	56.5	-3.765	0.07	2	34.078	0.567	17.919	0.265	-233	29	3.500	37.843
S.130	12.9	-14.2	1113.9	28.0	55.1	70.3	41.8	56.4	-3.961	0.03	3	35.909	0.515	18.692	0.254	-268	19	5.286	39.870
83-103	12.9	-12.4	1114.0	28.5	53.7	70.4	41.8	57.5	-4.329	0.03		30.499		15.855		-249		-0.024	34.828
S.138	12.9	-14.9	1127.1	27.7	56.8	70.9	42.4	56.6	-4.069	0.03	2	35.822	0.5	18.667	0.3	-247	5	5.138	39.891
S136	12.8	-14.7	1113.4	27.8	57.4	71.5	43.3	57.4	-4.023	0.02		33.422		17.355		-246		2.767	37.445
83-116	12.7	-12.2	1233.2	28.5	54.8	71.4	42.7	58.5	-4.316	0.03	2	31.084		16.149		-264		0.558	35.401
83-115	12.4	-12.3	1301.3	27.8	56.5	66.8	44.2	53.8	-4.170	0.01	2	31.524	0.4	16.418	0.2	-226	17	0.887	35.694
Wooded savana																			
83-8	14.9	-15.9	485.2	28.0	50.9	67.0	37.3	52.4	-3.948	0.16		36.813		19.167		-270		6.181	40.762
S7	14.8	-16.0	513.6	28.2	52.0	67.9	38.0	53.1	-4.263	0.26		29.491		15.331		-241		-1.076	33.755
83-4	14.7	-16.5	539.7	27.0	57.4	70.9	43.7	57.3	-3.821	0.43		26.127		13.565		-231		-4.665	29.948
82-77	14.6	-16.3	535.5	28.0	53.5	69.0	39.2	54.0	-3.798	0.14	2	35.214	0.8	18.312	0.4	-281	10	4.601	39.012
S91	13.6	-13.4	883.1	28.7	49.4	66.2	37.8	53.0	-3.984	0.40	2	34.512	0.2	18.009	0.1	-213	30	4.013	38.496
C4L8	13.5	-13.7	878.1	28.6	50.7	67.3	38.7	53.8	-3.984	0.13		32.302		16.850		-206		1.793	36.286
83-127	13.1	-14.1	1055.1	28.2	53.6	69.3	40.7	55.5	-3.785	0.49	2	35.638	0.2	18.573	0.1	-244	1	5.054	39.423
Enclosed savana																			
Biendi 1	-2.0	11.1	1839.0	25.9	80.9	80.9	67.4	67.4	-3.687	0.76		33.086	0.0	17.233	0.0	-205	20	2.096	36.773
Doubou	-1.8	10.9	1986.0	25.9	81.2	81.2	67.9	67.9	-3.631	1.58		31.931	0.6	16.665	0.3	-194	8	0.954	35.562
Humid forest																			
83-151	12.5	-16.6	1428.6	26.5	65.8	74.9	51.0	60.8	-3.787	6.78		33.097		17.288		-187		2.221	36.884
S155	12.5	-16.3	1352.6	27.0	64.4	74.3	49.4	59.9	-3.777	4.85	2	29.092	0.2	15.180	0.1	-181	4	-1.698	32.869
04-94		13.1	1676.4	24.3	81.4	81.4	65.8	65.8	-4.464	2.44	2	32.638	0.2	17.093	0.1	-140	4	1.371	37.102
04-88		12.4	1707.0	24.9	81.9	81.9	67.1	67.1	-4.458	5.45		33.137	0.4	17.345	0.2	-151	18	1.977	37.595
04-47	-0.2	12.3	1724.0	26.2	82.1	82.1	67.4	67.4	-1.515	3.48		32.953	0.0	17.215	0.0	-185	17	2.026	34.468
04-66	-0.2	12.5	1690.6	25.8	82.0	82.0	67.3	67.3	-4.354	1.84		29.959	0.6	15.641	0.3	-177	24	-1.040	34.314
04-65	-0.2	12.6	1690.6	25.8	82.0	82.0	67.3	67.3	-4.195	2.19		32.791	0.6	17.158	0.3	-156	25	1.791	36.985
04-118	-0.2	10.5	2148.4	26.4	82.5	82.5	69.2	69.2	-3.556	3.69		31.840	0.4	16.648	0.2	-164	4	0.945	35.396
Dimonik	-4.1	12.4	1286.6	24.7	80.3	80.3	68.1	68.1	-4.284	5.80		30.928		16.123		-205		-0.275	35.212
Outliers																			
RIM1	16.7	-16.0	216.4	26.7	52.3	72.2	39.4	58.6	-3.857	0.06		38.131		19.828		-305		7.264	41.987
C3L4	15.6	-14.2	362.0	29.3	41.8	59.1	30.3	45.0	-3.968	0.06		25.185	0.2	13.141	0.1	-157	10	-5.211	29.153

(1) Amount weighted average for months with at least one day with precipitation>0.1mm

Figure captions

Figure 1. Growth chamber experiment: a) ^{17}O-excess *vs* relative humidity (RH) of irrigation water (IW), soil water (SW), leaf water (LW) and phytolith (Phyto). Error bars show standard deviation (SD) on the replicates. They are smaller than the symbol when not shown. b) ^{18}O-enrichment from irrigation water to leaf water ($\Delta'^{18}O_{LW\text{-}IW}$), from irrigation water to phytolith ($\Delta'^{18}O_{Phyto\text{-}IW}$) and from leaf water to phytolith ($\Delta'^{18}O_{Phyto\text{-}LW}$). c) ^{17}O-excess associated with the enrichment from irrigation water to leaf water (^{17}O–excess$_{e\ LW\text{-}IW}$), from irrigation water to phytolith (^{17}O–excess$_{e\ Phyto\text{-}IW}$), and from leaf water to phytolith (^{17}O–excess$_{e\ Phyto\text{-}LW}$). d, e and f) linear correlations for the 40-80% RH range extracted from a, b and c, respectively.

Figure 2. Growth chamber experiment: phytolith types extracted from *Festuca arundinaceae* and observed in natural light microscopy: epidermal long cell (LC), epidermal short cell (SC).

Figure 3. Natural West and Central African transect: **δ**'^{18}O of phytoliths (**δ**'^{18}O$_{Phyto}$) *vs* relative humidity RH-rd0>1 (see fig. 4 for explanation). Error bars show standard deviation (SD) on the replicates. When not shown, they are smaller than the symbol.

Figure 4. Natural West and Central African transect: ^{17}O-excess *vs* relative humidity (RH) of phytolith assemblages from soil tops collected under savanna, wooded savanna, humid forest and enclosed savanna along a humidity gradient (Table 1). The growth chamber ^{17}O–excess$_{Phyto}$ *vs* RH correlation line is displayed for comparison. a) RH-Av: yearly average of monthly means; b) RH-rd0>1: yearly average of monthly means for months with at least one day with precipitation higher than 0.1mm; c) RH15: RH at 15:00 H UTC; d) RH15-rd0>1: RH-rd0>1 at 15:00 H UTC.

Figure 5. Natural West and Central African transect: ^{17}O-excess of phytoliths (^{17}O-excess$_{Phyto}$) *vs* d/p.

Figure 6. Growth chamber experiment: ^{17}O-excess *vs* δ'^{18}O of irrigation water (IW), soil water (SW), bulk leaf water (LW) and phytolith (Phyto). Error bars show standard deviation (SD) on the replicates. The leaf water line (blue) represents how the triple oxygen isotope composition of the bulk leaf water of *Festuca arundinacea* evolves from an irrigation water signature to a more evaporated water signature when RH decreases. Assuming that phytoliths precipitate from the bulk leaf water, the expected phytolith line (black) should be parallel to the leaf water line as the equilibrium fractionation between phytolith and leaf water is constant at constant temperature (25°C). In the investigated case this fractionation, represented by the black dotted line, is equivalent to $\lambda=0.522$ (table 1). The isotope signature of phytoliths formed at RH higher than 40% follow the expected phytolith line. However, the isotope signature of phytoliths formed at 40% RH suggest a forming water more evaporated than the bulk leaf water.

Figure 1

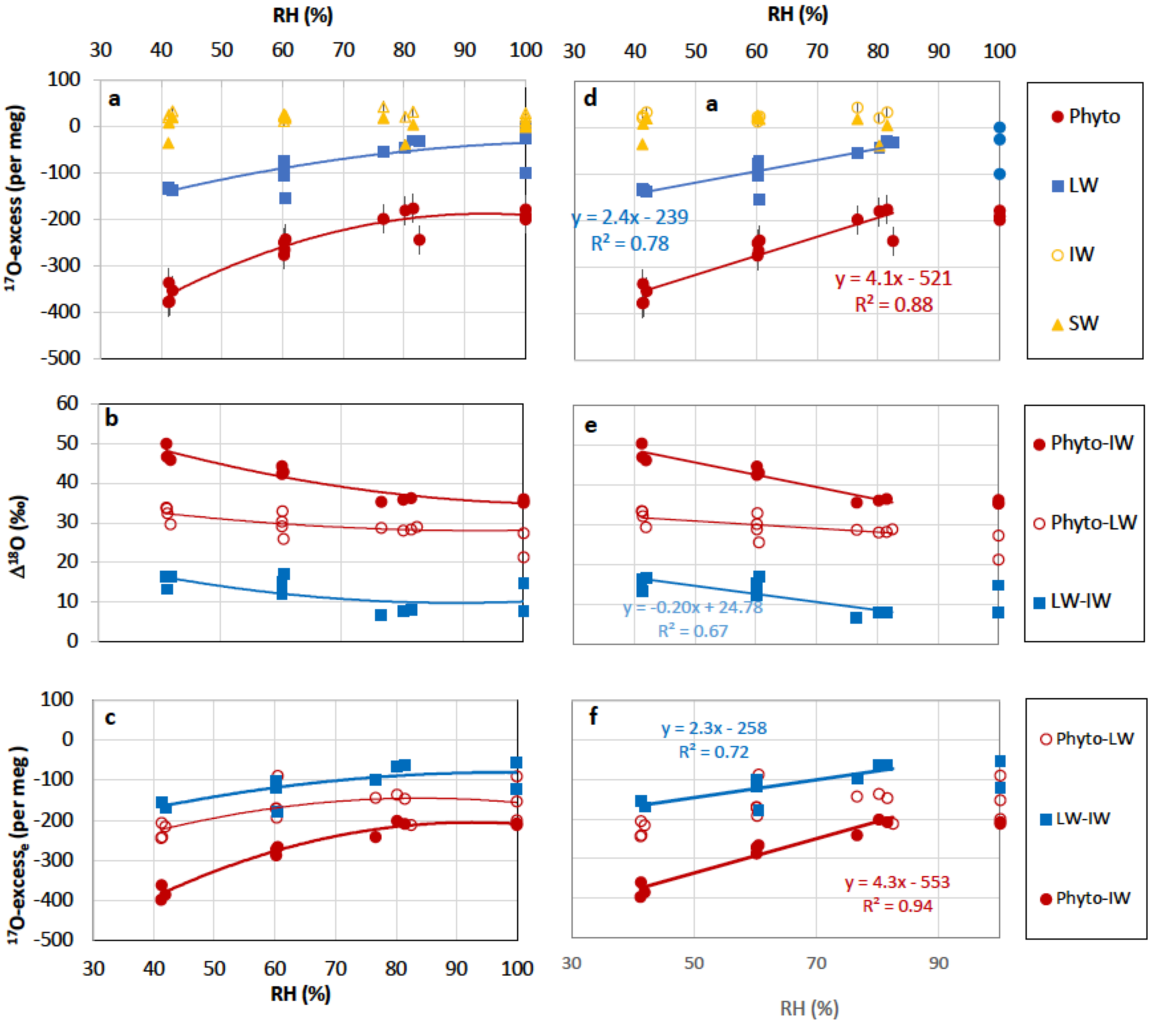
RH (%)
30 40 50 60 70 80 90 100
RH (%)
30 40 50 60 70 80 90 100
100 0 -100 -200 -300 -400 -500
^{17}O-excess (per meg)
a
d
a
y = 2.4x - 239
R² = 0.78
y = 4.1x - 521
R² = 0.88
● Phyto
■ LW
○ IW
▲ SW
60 50 40 30 20 10 0
Δ^{18}O (‰)
b
e
y = -0.20x + 24.78
R² = 0.67
● Phyto-IW
○ Phyto-LW
■ LW-IW
100 0 -100 -200 -300 -400 -500
^{17}O-excess$_e$ (per meg)
c
f
y = 2.3x - 258
R² = 0.72
y = 4.3x - 553
R² = 0.94
○ Phyto-LW
■ LW-IW
● Phyto-IW
30 40 50 60 70 80 90 100
RH (%)
30 50 70 90
RH (%)

Figure 2

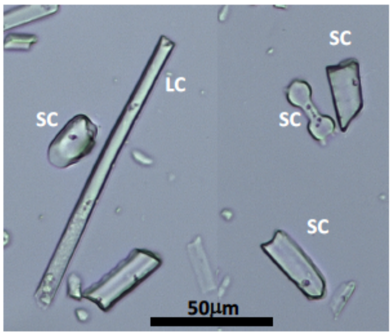

953

Figure 3

954

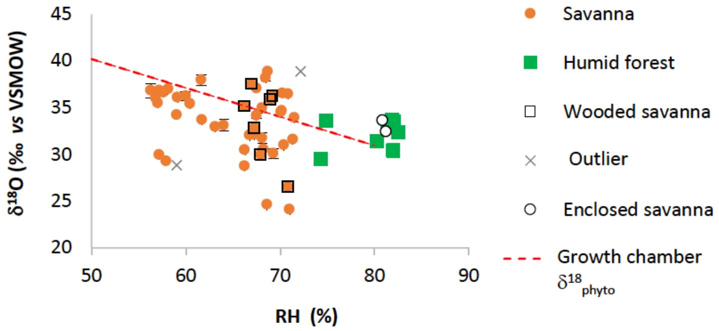

955

Figure 4

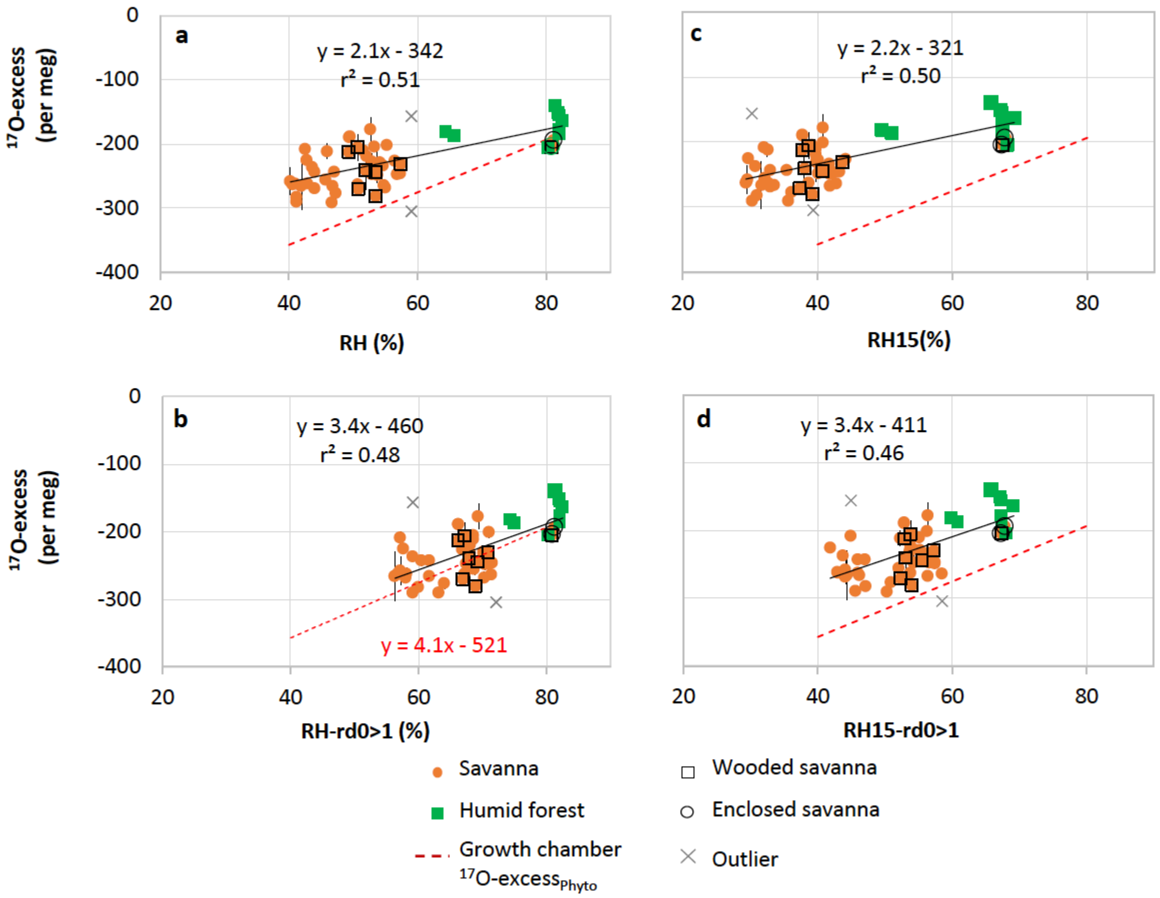
a
y = 2.1x - 342
r² = 0.51
c
y = 2.2x - 321
r² = 0.50
b
y = 3.4x - 460
r² = 0.48
y = 4.1x - 521
d
y = 3.4x - 411
r² = 0.46
¹⁷O-excess (per meg)
0
-100
-200
-300
-400
20
40
60
80
RH (%)
RH15(%)
RH-rd0>1 (%)
RH15-rd0>1
Savanna
Humid forest
Growth chamber ¹⁷O-excess Phyto
Wooded savanna
Enclosed savanna
Outlier

959

960

Figure 5

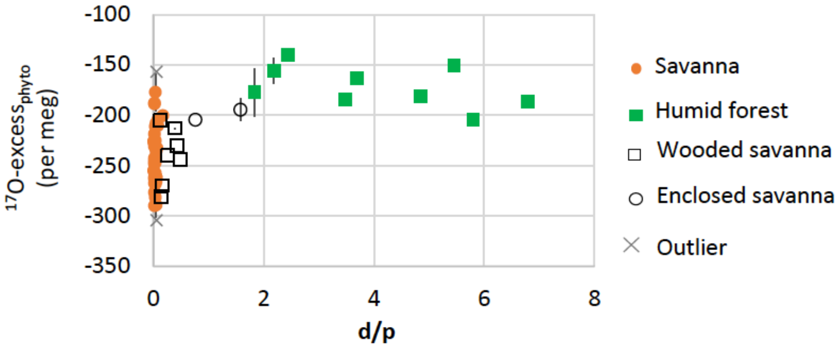

961

Figure 6

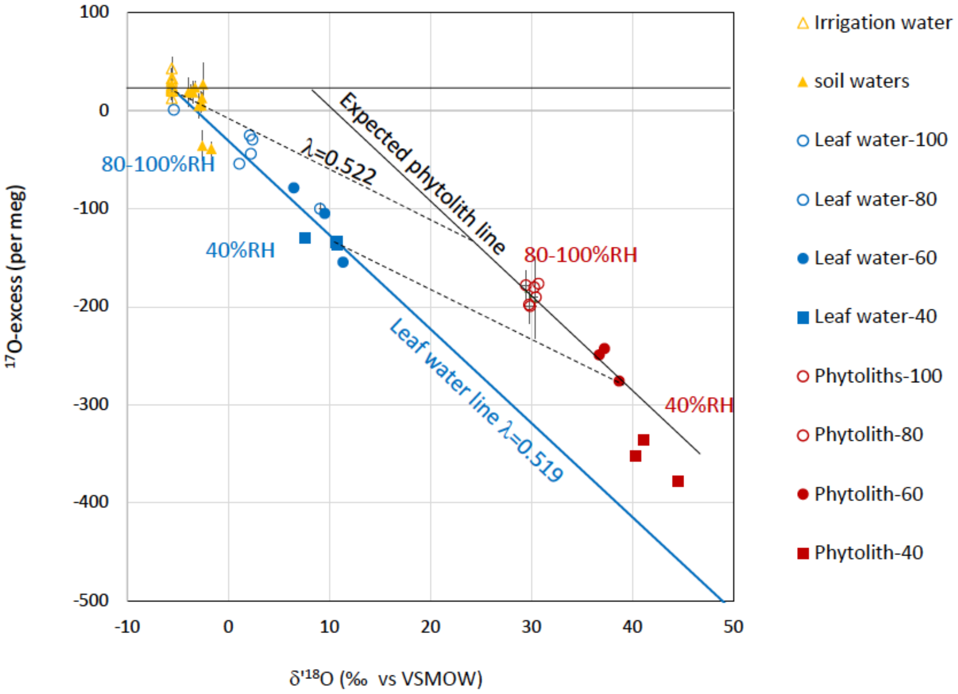

100
0
-100
-200
-300
-400
-500
-10
0
10
20
30
40
50
^{17}O-excess (per meg)
δ'^{18}O (‰ vs VSMOW)
80-100%RH
40%RH
λ=0.522
Expected phytolith line
80-100%RH
40%RH
Leaf water line λ=0.519
△ Irrigation water
▲ soil waters
○ Leaf water-100
○ Leaf water-80
● Leaf water-60
■ Leaf water-40
○ Phytoliths-100
○ Phytolith-80
● Phytolith-60
■ Phytolith-40

Table S1: a) Comparison between IRMS (4 replicates, SD of 0.015‰, 0.010‰ and 5 per meg for $\delta^{17}O$, $\delta^{18}0$ and ^{17}O-excess respectively) and laser analyser (12 replicates, SD displayed) measurements of working water standards. SD for standard deviation; **b)** Measurements of soil water samples with the isotope laser analyzer (Picarro L2140i) operated in ^{17}O-excess mode with and without the Picarro micro combustion module (MCM); SD: standard deviation calculated on the replicates.

a)

	Laser analyzer Picarro L2140i (Ecotron)			IRMS MAT 253 (LSCE)			Difference laser analyzer/IRMS		
	$\delta^{18}O$	**$\delta^{17}O$**	**^{17}O-excess**	**$\delta^{18}O$**	**$\delta^{17}O$**	**^{17}O-excess**	**$\delta^{18}O$**	**$\delta^{17}O$**	**^{17}O-excess**
	‰	‰	per meg	‰	‰	per meg	‰	‰	per meg
GIENS-1	-0.13	-0.07	1.11	-0.26	-0.14	-5.30	0.13	0.08	6.40
ECO-1	-5.68	-2.97	29.13	-5.61	-2.94	28.10	-0.07	-0.03	1.04
ICEBERG-1	-26.88	-14.25	36.09	-27.13	-14.38	35.43	0.24	0.13	0.66

b)

▨ WITHOUT MCM (3replicates)

☐ WITH MCM (3 replicates)

Sample	**$\delta^{18}O$**				**$\delta^{2}H$**				**$\delta^{17}O$**				**^{17}O-excess**			
		SD		SD		SD		SD		SD		SD		SD		
	‰		‰		‰		‰		‰		‰		per meg		per meg	
B3-100-10-05-16	-2.643	0.029	-2.607	0.010	-18.704	0.187	-18.580	0.019	-1.392	0.014	-1.365	0.009	4.1	3.4	12.7	5.8
B2-60-10-05-16	-3.495	0.014	-3.469	0.023	-23.750	0.082	-23.541	0.073	-1.835	0.010	-1.814	0.019	12.0	6.4	18.7	11.1
B3-100-03-06-16	-2.799	0.018	-2.766	0.022	-18.868	0.105	-18.894	0.185	-1.462	0.022	-1.457	0.019	16.7	12.7	4.8	7.4
M1-40-03-06-16	-5.605	0.020	-5.584	0.005	-31.737	0.077	-31.684	0.155	-2.938	0.012	-2.929	0.004	25.7	3.0	23.5	1.7
B1-85-10-05-16	-2.945	0.038	-2.901	0.010	-20.987	0.018	-20.925	0.050	-1.551	0.045	-1.528	0.008	4.7	25.4	4.8	12.1
B10-40-10-05-16	-2.726	0.029	-2.697	0.022	-19.891	0.071	-19.594	0.097	-1.434	0.030	-1.416	0.015	6.8	16.2	8.5	10.3
B1-40-03-06-16	-3.903	0.011	-3.895	0.005	-25.017	0.187	-24.959	0.025	-2.041	0.012	-2.040	0.009	21.6	6.4	18.9	10.7
		0.023		0.014		0.104		0.086		0.021		0.012		10.5		8.4

Table S2. Growth chamber experiment : measured δ^{18}O, δ^{17}O and ^{17}O-excess of irrigation water (IW), soil water, leaf water (LW) and phytoliths. Av : average ; n : number of replicates ; SD : standard deviation calculated on the replicates; n.v. : no value.

	Irrigation water							Soil water							Leaf water							Phytoliths							
Sample	δ^{18}O	SD	δ^{17}O	SD	n	δ'^{18}O	^{17}O-excess	δ^{18}O	SD	δ^{17}O	SD	n	δ'^{18}O	^{17}O-excess	δ^{18}O	SD	δ^{17}O	SD	n	δ'^{18}O	^{17}O-excess	δ^{18}O	SD	δ^{17}O	SD	n	δ'^{18}O	^{17}O-excess	SD
	‰		‰			‰	per meg	‰		‰			‰	per meg	‰		‰			‰	per meg	‰		‰			‰	per meg	
P1-40-29-04-16	-5.546	0.017	-2.912	0.013	3	-5.562	20	-2.562	0.026	-1.389	0.029	3	-2.565	36	10.733	0.106	5.519	0.082	2	10.676	-133	45.454	0.212	23.361	0.152	2	44.451	-378	41
P10-40-10-05-16	-5.594	18.139	-2.933	16.016	3	-5.610	25	-2.697	0.022	-1.416	0.015	3	-2.701	9	7.590		3.870		1	7.561	-130	41.947	0.348	21.590	0.199	2	41.091	-336	15
P1-40-20-05-16	-5.580	0.019	-2.917	0.019	3	-5.596	33	-3.658	0.013	-1.913	0.013	3	-3.665	20	10.807		5.554		1	10.749	-137	41.150	0.592	21.161	0.291	2	40.326	-352	18
P1-40-03-06-16	n.v.		n.v.			n.v.	n.v.	n.v.		n.v.			n.v.	n.v.	8.530		4.360		1	8.494	-135	41.758		21.451		1	40.909	-376	
Av.						**-5.589**	**26**						**-2.977**	**21**						**9.370**	**-134**						**41.694**	**-360**	
SD						**0.025**	**6**						**0.600**	**14**						**1.596**	**3**						**1.867**	**20**	
P10-60-29-04-16	-5.564	0.007	-2.929	0.008	3	-5.579	13	-2.504	0.067	-1.296	0.057	3	-2.507	27	9.581	0.015	4.942	0.008	2	9.535	-104	39.426	0.528	20.346	0.255	4	38.669	-275	23
P2-60-10-05-16	-5.563	0.001	-2.917	0.016	3	-5.579	24	-3.469	0.023	-1.814	0.019	3	-3.475	19	11.370		5.832		1	11.306	-154	37.883	0.340	19.579	0.184	4	37.183	-243	4
P10-60-20-05-16	-5.566	0.021	-2.920	0.027	3	-5.582	23	-3.260	0.028	-1.699	0.008	3	-3.266	23	6.453		3.323		1	6.432	-78	37.368	0.504	19.306	0.257	2	36.687	-249	4
P10-60-03-06-16	n.v.		n.v.			n.v.	n.v.	n.v.		n.v.					2.488		1.241		1	2.485	-72	36.034		18.597		1	35.400	-265	
Av.						**-5.580**	**20**						**-3.083**	**23**						**7.440**	**-102**						**36.985**	**-258**	
SD						**0.002**	**6**						**0.509**	**4**						**3.869**	**37**						**1.351**	**15**	
P2-85-29-04-16	-5.594	0.014	-2.937	0.001	3	-5.610	21	-1.667	0.016	-0.920	0.010	3	-1.668	7	2.219	0.067	1.127	0.050	2	2.217	-44	30.718	0.385	15.920	0.212	3	30.255	-180	7
P1-85-10-05-16	-5.542	22.510	-2.898	22.807	3	-5.558	33	-2.901	0.010	-1.528	0.008	3	-2.905	5	2.402		1.238		1	2.399	-30	31.151	0.206	16.149	0.122	3	30.675	-176	1
P2-85-20-05-16	-5.561	0.014	-2.897	0.018	3	-5.577	43	-3.975	0.018	-2.082	0.010	3	-3.983	19	1.103		0.528		1	1.102	-54	30.218	0.070	15.642	0.036	2	29.770	-198	15
P2-85-03-06-16	n.v.		n.v.			n.v.	n.v.	n.v.				3			0.802		0.391		1	0.802	-32	30.134	0.252	15.552	0.090	2	29.689	-244	
Av.						**-5.581**	**32**						**-2.852**	**9**						**1.630**	**-40**						**30.098**	**-199**	
SD						**0.026**	**11**						**1.158**	**8**						**0.796**	**11**						**0.459**	**31**	
P3-100-10-05-16	-5.582	0.034	-2.930	0.028	3	-5.597	21	-2.607	0.010	-1.365	0.009	3	-2.611	13	9.125	1.955	4.707	0.986	2	9.084	-100	30.876	0.027	15.992	0.003	2	30.409	-190	17
P3-100-20-05-16	-5.572	10.963	-2.916	6.038	3	-5.588	29	-2.677	0.015	-1.409	0.007	3	-2.680	6	2.121		1.094		1	2.119	-25	29.901	0.148	15.497	0.071	3	29.463	-178	6
P3-100-03-06-16	n.v.		n.v.			n.v.	n.v.	n.v.		n.v.			n.v.	n.v.	-5.382		-2.844		1	-5.396	1	30.286		15.676		1	29.837	-199	
Av.						**-5.593**	**25**						**-2.646**	**9**						**1.935**	**-41**						**29.903**	**-189**	
SD						**0.007**	**5**						**0.049**	**5**						**7.242**	**53**						**0.477**	**11**	
Av.(a)						**-5.586**	**26**						**-2.889**	**16**															
SD (a)						**0.006**	**5**						**0.188**	**8**															

(a) Calculated on the raw values.

Table S3. Growth chamber experiment: predicted isotopic enrichment in ^{18}O from irrigation water to leaf water (Δ^{18}_{LW-IW}) after Cernusak et al. (2016 ; Additional Supporting information). Refer to Cernusak et al. (1996) for symbol and calculations used in the table. Added calculations are displayed in grey columns: Δ^{17}_{LW-IW} and ^{17}O-excess$_e$ were calculated using $^{17}\alpha_{eq} = {}^{18}\alpha_{eq}{}^{0.529}$ and $^{17}\alpha_k = {}^{18}\alpha_{eq}{}^{0.518}$, for the equilibrium fractionation and kinetic fractionation, respectively. $\lambda_{LW-IW} = \Delta'^{17} / \Delta'^{18}$. IW: irrigation water; LW : leaf water (LW).

	Sampling details			Physiological data		Isotopic data						Calculations																			
																					Predicted						Observed				
Sample	Air tem.	Leaf temp.	Air RH	Stomatal cond.	Boundary layer cond.	Atm. vapor δ^{18}O	Atm. vapor δ^{17}O	IW δ^{18}O	IWδ^{17}O	LW δ^{18}O	LW δ^{17}O	air vapor pressure- e_a	leaf vapor pressure- e_i	w_a/w_i	ε_k for δ^{18}O	ε_k for δ^{17}O	ε^* for δ^{18}O at leaf temp	ε^* for δ^{17}O at leaf temp	Δ_v for δ^{18}O	Δ_v for δ^{17}O	Δ^{18}_{LW-IW}	Δ^{17}_{LW-IW}	Δ'^{18}_{LW-IW}	Δ'^{17}_{LW-IW}	^{17}O-excess$_e$ LW-IW	λ_{LW-IW}	Δ^{18}_{LW-IW}	Δ'^{18}_{LW-IW}	Δ'^{17}O$_{LW-IW}$	^{17}O-excess$_e$ LW-IW	λ_{LW-IW}
	°C	°C	%	mol m^{-2} s^{-1}	mol m^{-2} s^{-1}	‰	‰	‰	‰	‰	‰	kPa	kPa		‰	‰	‰	‰	‰	‰	‰		‰	‰	per meg		‰	‰	‰	per meg	
P1-40-29-04-16	25.0	25.0	41.2	0.031	2	-5.55	-2.91	-5.55	-2.91	10.73	5.52	1.31	3.18	0.41	27.860	14.336	9.386	4.954	0.000	0.000	25.922	13.426	25.591	13.336	-176	0.521	16.370	16.238	8.420	-154	0.519
P10-40-10-05-16	25.0	25.0	41.3	0.032	2	-5.59	-2.93	-5.59	-2.93	7.59	3.87	1.31	3.18	0.41	27.860	14.336	9.386	4.954	0.000	0.000	25.893	13.411	25.564	13.322	-176	0.521	13.259	13.171	6.799	-155	0.516
P1-40-20-05-16	25.0	25.0	41.9	0.032	2	-5.58	-2.92	-5.58	-2.92	10.81	5.55	1.33	3.18	0.42	27.857	14.334	9.386	4.954	0.000	0.000	25.723	13.324	25.398	13.236	-174	0.521	16.479	16.345	8.460	-170	0.518
P1-40-03-06-16	25.0	25.0	41.4	0.032	2	n.v.	n.v.	n.v.	n.v.	8.53	4.36	1.32	3.18	0.41	27.860	14.336	9.386	4.954	n.v.	n.v.											
P10-60-29-04-16	25.0	25.0	60.5	0.052	2	-5.56	-2.93	-5.56	-2.93	9.58	4.94	1.92	3.18	0.61	27.770	14.290	9.386	4.954	0.000	0.000	20.458	10.627	20.252	10.571	-122	0.522	15.230	15.115	7.864	-117	0.520
P2-60-10-05-16	25.0	25.0	60.2	0.052	2	-5.56	-2.92	-5.56	-2.92	11.37	5.83	1.91	3.18	0.60	27.772	14.291	9.386	4.954	0.000	0.000	20.543	10.670	20.335	10.614	-123	0.522	17.028	16.885	8.737	-178	0.517
P10-60-20-05-16	25.0	25.0	60.5	0.052	2	-5.57	-2.92	-5.57	-2.92	6.45	3.32	1.92	3.18	0.61	27.770	14.290	9.386	4.954	0.000	0.000	20.458	10.627	20.252	10.571	-122	0.522	12.087	12.014	6.242	-101	0.520
P10-60-03-06-16	25.0	25.0	60.3	0.052	2	n.v.	n.v.	n.v.	n.v.	2.49	1.24	1.92	3.18	0.60	27.771	14.291	9.386	4.954	n.v.	n.v.											
P2-85-29-04-16	25.0	25.0	80.2	0.074	2	-5.59	-2.94	-5.59	-2.94	2.22	1.13	2.55	3.18	0.80	27.680	14.244	9.386	4.954	0.000	0.000	14.918	7.789	14.808	7.758	-60	0.524	7.857	7.826	4.067	-65	0.520
P1-85-10-05-16	25.0	25.0	76.6	0.070	2	-5.54	-2.90	-5.54	-2.90	2.40	1.24	2.44	3.18	0.77	27.697	14.252	9.386	4.954	0.000	0.000	15.928	8.306	15.802	8.272	-72	0.523	7.989	7.957	4.139	-62	0.520
P2-85-20-05-16	25.0	25.0	81.5	0.075	2	-5.56	-2.90	-5.56	-2.90	1.10	0.53	2.59	3.18	0.82	27.675	14.241	9.386	4.954	0.000	0.000	14.554	7.602	14.449	7.573	-56	0.524	6.702	6.679	3.429	-97	0.513
P2-85-03-06-16	25.0	25.0	82.5	0.076	2	n.v.	n.v.	n.v.	n.v.	0.80	0.39	2.62	3.18	0.83	27.670	14.239	9.386	4.954	n.v.	n.v.											
P3-100-10-05-16	25.0	25.0	100.0	0.095	2	*-5.58*	*-2.93*	*-5.58*	*-2.93*	9.13	4.71	3.18	3.18	1.00	27.592	14.199	9.386	4.954	0.000	0.000	9.386	4.954	9.342	4.942	9	0.529	14.789	14.681	7.630	-122	0.520
P3-100-20-05-16	25.0	25.0	100.0	0.095	2	-5.57	-2.92	-5.57	-2.92	2.12	1.09	3.18	3.18	1.00	27.592	14.199	9.386	4.954	0.000	0.000	9.386	4.954	9.342	4.942	9	0.529	7.736	7.706	4.014	-54	0.521
P3-100-03-06-16	25.0	25.0	100.0	0.095	2	n.v.	n.v.	n.v.	n.v.	-5.38	-2.84	3.18	3.18	1.00	27.592	14.199	9.386	4.954	n.v.	n.v.											

Stomatal conductance: gs ranges from 0.1 to 0.5 in investigated C3 grasses is lower than 0.2 in C4 grasses. Cf Ocheltree et al., 2012. Here gs is calculated according to Liet al., 2017.

Boundary layer cond: 0.2 to 3 in Li et al., 2017